iScience

CellPress
OPEN ACCESS

Article

Robust GRK2/3/6-dependent desensitization of oxytocin receptor in neurons

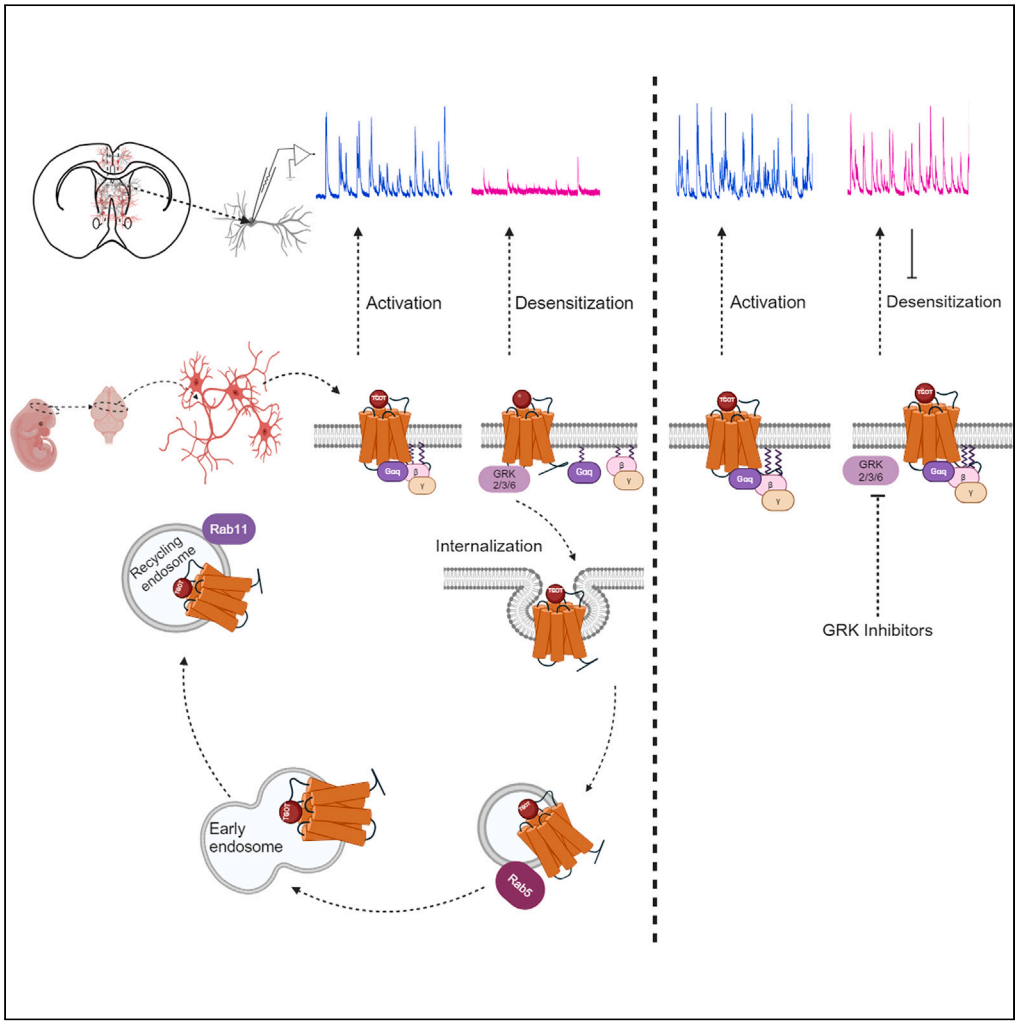

Kiran George, Hanh T.M. Hoang, Taryn Tibbs, Raghavendra Y. Nagaraja, Guangpu Li, Eva Troyano-Rodriguez, Mohiuddin Ahmad

mohiuddin-ahmad@ouhsc.edu

Highlights

Agonist-induced desensitization and internalization of OXTR in mouse brain neurons

GRK2/3/6 recruited to neuronal OXTR and required for desensitization and internalization

β-arrestin-1 and β-arrestin-2 appear redundant for neuronal OXTR desensitization

Neuronal OXTR trafficking to early endosomes is dependent on Rab5

George et al., iScience 27, 110047
June 21, 2024
https://doi.org/10.1016/j.isci.2024.110047

iScience

CellPress
OPEN ACCESS

Article

Robust GRK2/3/6-dependent desensitization of oxytocin receptor in neurons

Kiran George,[1,3] Hanh T.M. Hoang,[1,3] Taryn Tibbs,[1] Raghavendra Y. Nagaraja,[1] Guangpu Li,[2] Eva Troyano-Rodriguez,[1] and Mohiuddin Ahmad[1,4,*]

SUMMARY

Oxytocin plays critical roles in the brain as a neuromodulator, regulating social and other affective behavior. However, the regulatory mechanisms controlling oxytocin receptor (OXTR) signaling in neurons remain unexplored. In this study, we have identified robust and rapid-onset desensitization of OXTR response in multiple regions of the mouse brain. Both cell autonomous spiking response and presynaptic activation undergo similar agonist-induced desensitization. G-protein-coupled receptor kinases (GRK) GRK2, GRK3, and GRK6 are recruited to the activated OXTR in neurons, followed by recruitment of β-arrestin-1 and -2. Neuronal OXTR desensitization was impaired by suppression of GRK2/3/6 kinase activity but remained unaltered with double knockout of β-arrestin-1 and -2. Additionally, we observed robust agonist-induced internalization of neuronal OXTR and its Rab5-dependent recruitment to early endosomes, which was impaired by GRK2/3/6 inhibition. This work defines distinctive aspects of the mechanisms governing OXTR desensitization and internalization in neurons compared to prior studies in heterologous cells.

INTRODUCTION

Oxytocin acts as a neuromodulator in the brain to regulate various facets of social, sexual, and anxiety-related behavior.[1–3] This is in addition to its role as a hormone to stimulate contraction of the uterine myometrium during parturition and mammary gland myoepithelium during lactation. Oxytocin binds to and activates primarily the oxytocin receptor (OXTR), a G-protein-coupled receptor (GPCR), to initiate intracellular signaling.[4] Multiple studies have reported single nucleotide polymorphisms, heterozygous deletion, and abnormal promoter methylation in the oxytocin receptor gene (*OXTR*) in patients with autism spectrum disorder (ASD).[5–7] The association is also supported by animal studies as *Oxtr* knockout mice recapitulate several features of ASD and show impairments in social preference, social memory, and social communication (ultrasonic vocalization).[8–12] In light of these findings, there is tremendous interest in understanding OXTR function and signaling in the brain. Investigations at the circuit level have identified the role of oxytocin in regulating excitatory and inhibitory synaptic transmission, neuronal spiking, and synaptic plasticity in various brain regions.[13–18] However, the molecular mechanisms that mediate and regulate OXTR signaling intracellularly within neurons remain largely unexplored.

An important regulatory process for GPCR signaling is agonist-induced desensitization in which the activated receptors lose the ability to further respond to the agonist for extended periods of time.[19–21] This process dampens and curtails receptor signaling, thus preventing excessive activation of cellular pathways. The desensitization of GPCR response can occur at the level of receptors through uncoupling of G proteins and/or internalization of the activated receptor.[22,23] It can also be contributed by inactivation of downstream signaling pathways or effector channels.[24,25] Each of these processes contribute differentially to the desensitization of different GPCRs. Importantly, the mechanisms may differ between cell types for each GPCR,[26,27] which makes it critical to systematically study receptor desensitization in different tissues in which the GPCR is natively expressed. The process of desensitization for OXTR has primarily been studied in heterologous cell lines such as HEK293 cells with transfected OXTR. This work showed that the process involves the phosphorylation of agonist-bound OXTR by G-protein-coupled receptor kinase 2 (GRK2), which is followed by the recruitment of β-arrestin-1 and -2 and consequently receptor desensitization[28,29] and internalization.[30,31] In uterine myometrial cells, knocking down GRK6, but not GRK2, impaired OXTR desensitization,[32] thus highlighting cell-specific differences. In addition, knocking down β-arrestin-1 or -2 reduced OXTR desensitization by half in these cells.[33] Apart from a few reports on OXTR desensitization in particular rat brain regions,[34,35] very little is known about this process in the mammalian brain with underlying mechanisms remaining unexplored in neurons.

[1]Department of Cell Biology, University of Oklahoma Health Sciences Center, Oklahoma City, OK 73104, USA
[2]Department of Biochemistry and Physiology, University of Oklahoma Health Sciences Center, Oklahoma City, OK 73104, USA
[3]These authors contributed equally
[4]Lead contact
*Correspondence: mohiuddin-ahmad@ouhsc.edu
https://doi.org/10.1016/j.isci.2024.110047

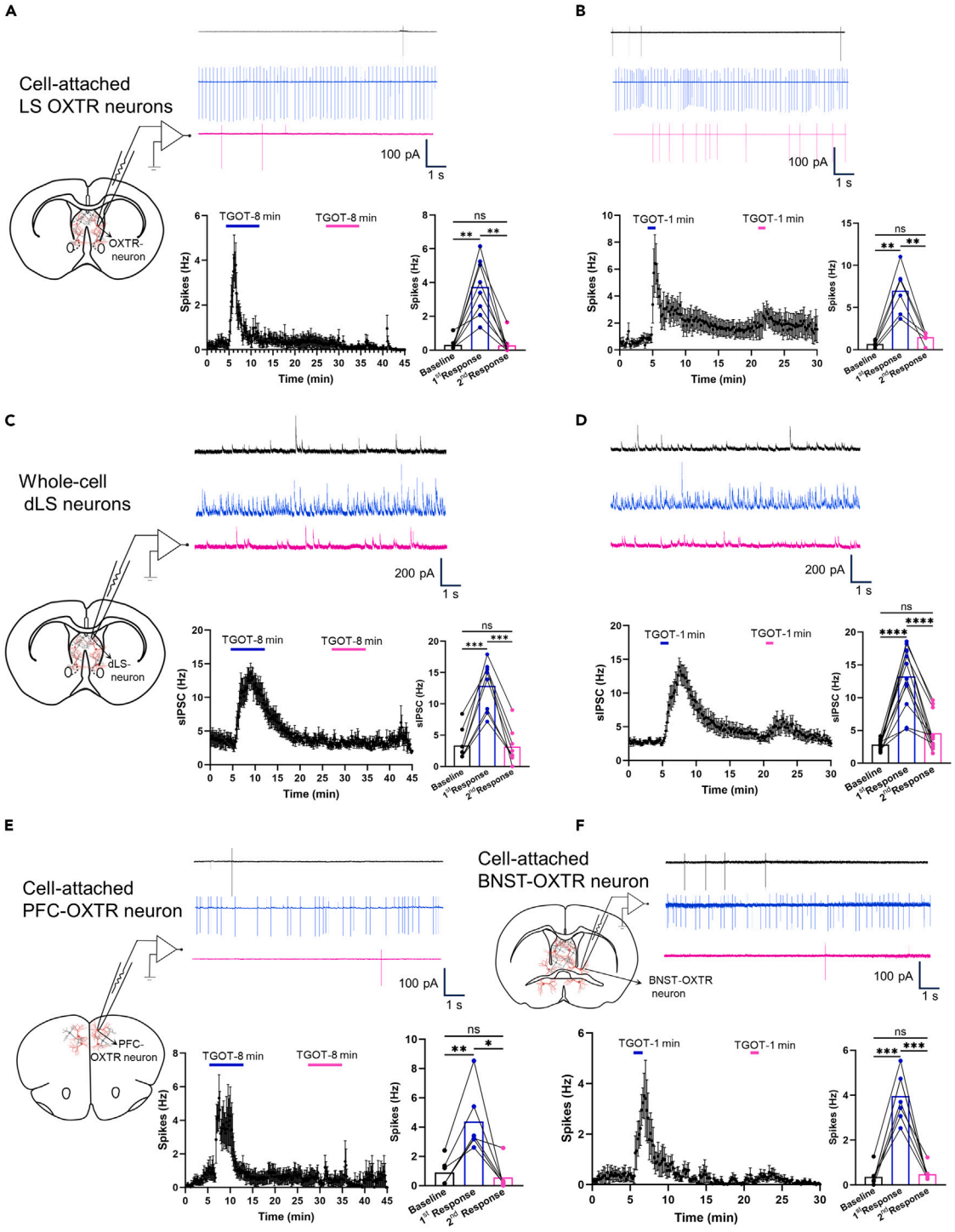

Figure 1. Robust agonist-induced desensitization of OXTR response in the mouse brain

(A) Cell-attached recordings from OXTR neurons in the LS (schematic on left) showing spikes in response to two sequential applications of 200 nM TGOT for 8 min each separated by 15 min. Sample traces (top) are shown for recordings during baseline (black), first application (blue), and second application (magenta). Summary graph of the time course (bottom left) and bar graphs with spike frequency at baseline, peak of first and peak of second response (bottom right) are also shown in this and subsequent panels. Spike frequency (Hz): baseline, 0.307 $\pm$ 0.130; 1st response, 3.738 $\pm$ 0.594; 2nd response, 0.281 $\pm$ 0.202; n = 8 cells, 4 mice.

(B) Cell-attached recordings from OXTR neurons in the LS showing spikes in response to two sequential applications of 200 nM TGOT for 1 min separated by 15 min. Spike frequency (Hz): baseline, 0.697 $\pm$ 0.158; 1st response, 7.000 $\pm$ 1.142; 2nd response, 1.506 $\pm$ 0.273; n = 6 cells, 3 mice.

Figure 1. *Continued*

(C) Whole-cell recordings of sIPSC from dorsal LS neurons showing response to two applications of 200 nM TGOT for 8 min each. sIPSC frequency (Hz): baseline, 3.350 ± 0.883; 1st response, 12.890 ± 1.410; 2nd response, 3.187 ± 1.006; n = 8 cells, 4 mice.

(D) Whole-cell recordings of sIPSC from dorsal LS neurons showing response to two applications of 200 nM TGOT for 1 min separated by 15 min (*n* = 12 cells). sIPSC frequency (Hz): baseline, 2.849 ± 0.210; 1st response, 13.250 ± 1.360; 2nd response, 4.608 ± 0.814; n = 12 cells, 6 mice.

(E) Cell-attached recordings from OXTR neurons in the PFC showing spikes in response to two sequential applications of 200 nM TGOT for 8 min each separated by 15 min. Spike frequency (Hz): baseline, 0.898 ± 0.377; 1st response, 4.389 ± 0.917; 2nd response, 0.561 ± 0.403; n = 6 cells, 4 mice.

(F) Cell-attached recordings from OXTR neurons in the BNST showing spikes in response to two sequential applications of 200 nM TGOT for 1 min each separated by 15 min. Spike frequency (Hz): baseline, 0.369 ± 0.158; 1st response, 3.962 ± 0.404; 2nd response, 0.486 ± 0.128; n = 7 cells, 4 mice. The data in graphs are shown as mean ± SEM. *p < 0.05, **p < 0.01, ***p < 0.001, ****p < 0.0001, repeated measures one-way ANOVA with post-hoc Tukey's multiple comparisons test.

We now report robust desensitization of OXTR response following its activation in multiple regions of the mouse brain including the lateral septum (LS), prefrontal cortex (PFC), and bed nucleus of stria terminalis (BNST). We identify that the desensitization occurs at the level of G proteins in neurons and is associated with recruitment of GRK2, GRK3, and GRK6 as well as β-arrestin-1 and -2 to activated neuronal OXTR. We find that the knockout of β-arrestin-1 and -2 has no effect on OXTR desensitization in LS neurons, whereas inhibition of GRK2/3/6 leads to impairment of this process. We further show rapid-onset and prominent agonist-induced internalization of OXTR in neurons that is followed by recruitment to early endosomes in a Rab-5-dependent manner. The internalization is dependent on GRK2/3/6 kinase activity, but these GRK isoforms are individually redundant in this process. These results unravel specific mechanisms underlying the regulation of OXTR signaling in mouse brain neurons and lay the foundation for strategies to prolong oxytocin signaling to alleviate social deficits in neuropsychiatric disorders.

RESULTS

Agonist-induced desensitization of OXTR response in the LS of mouse brain

We started our investigation of OXTR desensitization in the mouse brain by performing electrophysiological recordings in acute brain slices in the LS. The LS receives axonal projections from hypothalamic oxytocin neurons and contains a distinct population of neurons expressing OXTR.[36–38] The role of OXTR in the LS in regulating social and fear-related behavior has been extensively documented and places the LS as a prominent node of oxytocin action in regulating behavioral outcomes.[39–43] To analyze the kinetics of agonist-induced OXTR response, we obtained cell-attached, loose-seal recordings from fluorescent (tdTomato-expressing) OXTR neurons in the LS of Oxtr-IRES-Cre;Ai14 mice (Figure S1A). To selectively activate OXTR, we used [Thr^4,Gly^7]oxytocin (TGOT), an analogue of oxytocin that is highly selective for the rodent OXTR with >600-fold affinity to OXTR compared to vasopressin receptors.[44] Bath application of 200 nM TGOT for 8 min led to an increase in spike frequency (in ~80% of recorded cells), which peaked within 2 min of onset and thereafter decreased to baseline in the continued presence of the agonist, suggesting acute desensitization of the OXTR response (Figure 1A). Following a 15-min washout, the second application of 200 nM TGOT produced no increase in spike frequency, indicating robust tachyphylaxis of the OXTR response (Figure 1A). We then assessed whether a shorter activation of OXTR would induce desensitization by applying 200 nM TGOT for 1 min followed 15 min later with a second application. The first agonist application produced a strong spiking response but the response to the second exposure was minimal, indicating strong desensitization (Figure 1B).

To complement the above analysis, we recorded spontaneous inhibitory postsynaptic currents (sIPSC) from neurons in the dorsal LS, which were identified in our experiments to receive inhibitory projections from OXTR neurons located in the intermediate LS (Figures S2A and S2B). Bath application of 200 nM TGOT for 8 min (Figure 1C) or 1 min (Figure 1D) resulted in a large increase in sIPSC frequency from the baseline during the first application but induced minimal or no increase when applied the second time, 15 min later. The response recorded from dorsal LS neurons was due to an upstream action of TGOT on OXTR neurons as it was blocked by tetrodotoxin (Figure S2A).

In the experiments described earlier, we applied TGOT at a concentration of 200 nM for either 1 or 8 min, consistent with the concentrations and durations commonly employed in *ex vivo* studies in the rodent brain.[13,14,16,18] To investigate whether desensitization is influenced by agonist concentration, we administered 10 or 50 nM of TGOT to LS slices in two sequential applications for 1 min each and recorded the responses from dorsal LS neurons. We found that 50 nM TGOT induced a similar level of desensitization as observed with the 200 nM concentration (Figure S2C). However, we were unable to assess the extent of desensitization induced by 10 nM TGOT because, at this concentration, the agonist failed to elicit any response. These findings suggest that desensitization occurs in LS neurons in our recording conditions as long as there is activation of a detectable OXTR response. To make sure that the lack of second response to the agonist is not due to the deteriorating health of the slice, we applied TGOT (200 nM, 1 min) later during the recording, at the time point matching the second application of the agonist in our previous experiments (Figure S2D). We observed strong response in the LS, confirming the viability and responsiveness of the cells for the duration of the recordings.

We next evaluated whether oxytocin, the endogenous agonist of OXTR, induces similar desensitization in LS neurons. Since oxytocin is an efficacious agonist on vasopressin AVPR1a receptors expressed in the LS,[43,45,46] we applied oxytocin in the presence of AVPR1a antagonist (d(CH$_2$)$_5^1$,Tyr(Me)^2,Arg^8)-Vasopressin, to selectively induce OXTR response. We used this antagonist at 25 nM concentration, which is in between its IC50 values of 5 and 30 nM for AVPR1a and OXTR, respectively. Recordings of sIPSC from the dorsal LS neurons revealed robust desensitization to sequential application of 200 nM oxytocin (Figure S3A). We repeated the experiment with oxytocin application combined with a second AVPR1a antagonist SR49059 (10 nM) and obtained similar desensitization (Figure S3B). Overall, our results suggest that OXTR are robustly desensitized following activation by oxytocin or its synthetic analog TGOT in the mouse brain LS.

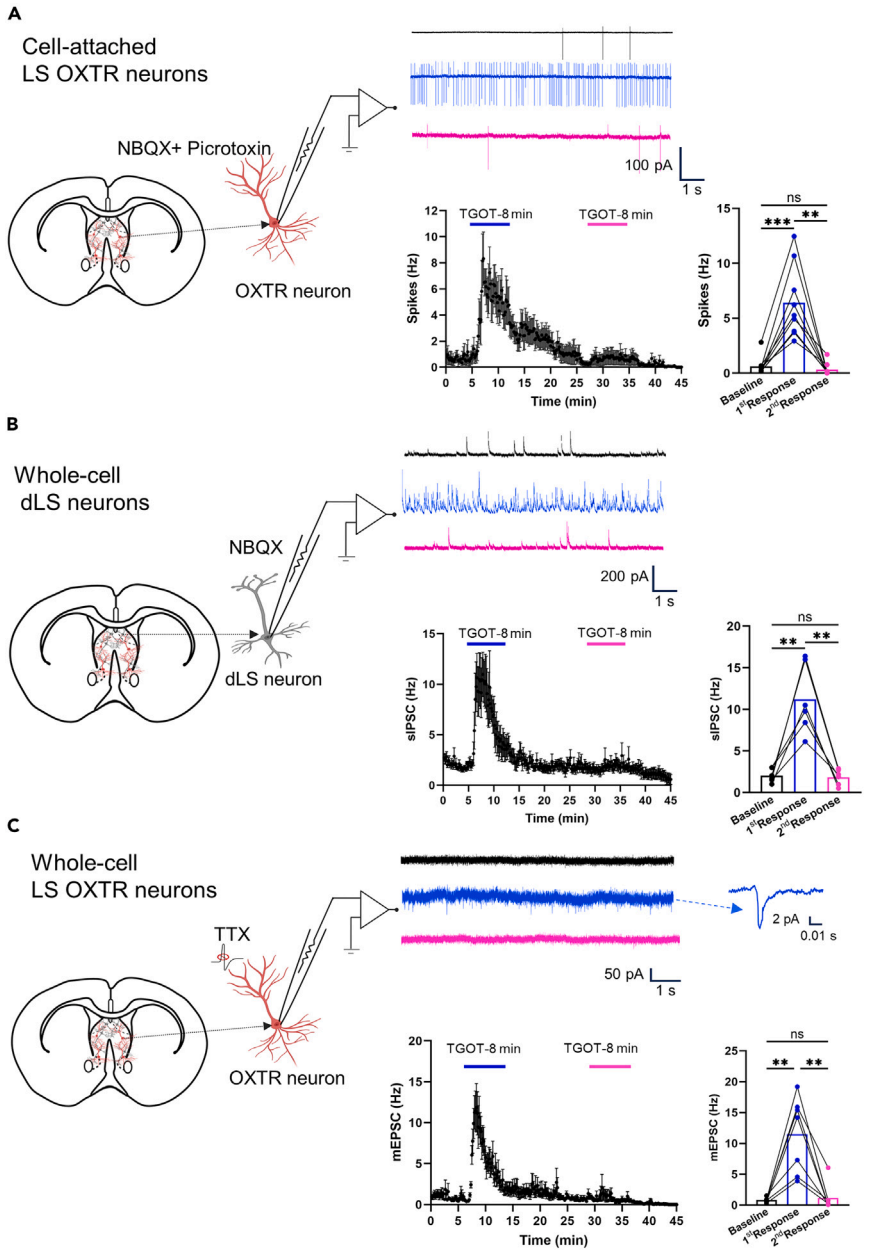

Figure 2. OXTR-induced spiking and presynaptic release responses undergo desensitization

(A) Cell-attached recordings from OXTR neurons in the LS in the presence of NBQX and picrotoxin (schematic on left) showing cell-autonomous spikes in response to two sequential applications of 200 nM TGOT for 8 min each separated by 15 min. Sample traces (top middle), summary graph of time course (bottom middle), and bar graphs with baseline, first peak response, and second peak response (right) are shown in this and subsequent panels. Spike frequency (Hz): baseline, 0.617 ± 0.284; 1st response, 6.404 ± 1.093; 2nd response, 0.344 ± 0.186; n = 9 cells, 5 mice.

(B) Whole-cell recordings of sIPSC from dorsal LS neurons in the presence of NBQX in response to two sequential applications of 200 nM TGOT for 8 min each separated by 15 min. The responses indicate cell-autonomous activation of OXTR neurons in the LS. sIPSC frequency (Hz): baseline, 2.047 ± 0.336; 1st response, 11.210 ± 1.693; 2nd response, 1.861 ± 0.384; n = 6 cells, 3 mice.

(C) Whole-cell recordings of mEPSC from OXTR neurons in the LS in response to two sequential applications of 200 nM TGOT for 8 min each separated by 15 min. The responses indicate presynaptic activation of OXTR on excitatory inputs to LS OXTR neurons. mEPSC frequency (Hz): baseline, 0.925 ± 0.136; 1st response, 12.770 ± 2.286; 2nd response, 1.656 ± 1.290; n = 7 cells, 6 mice. The data in graphs are shown as mean ± SEM. **p < 0.01, ****p < 0.0001, repeated measures one-way ANOVA with post-hoc Tukey's multiple comparisons test.

Agonist-induced desensitization of OXTR response in the PFC and BNST of mouse brain

To investigate whether agonist-induced desensitization of OXTR response is uniquely present in LS neurons or is a widespread feature in the mouse brain, we recorded spikes in cell-attached mode from visually identified OXTR neurons in the prefrontal cortex (PFC) and bed nucleus of stria terminalis (BNST) (Figures 1C and S1B). OXTR has been reported to be present in a subset of pyramidal neurons and interneurons in the PFC.[47,48] Application of TGOT (200 nM, 8 min) caused an increase in spike frequency in PFC OXTR neurons when applied *de novo* but had no effect when applied the second time after washout of 15 min (Figure 1E). Similarly, the OXTR response was strongly desensitized following TGOT application (200 nM, 1 min) in OXTR neurons localized in BNST (Figure 1F). These results suggest that OXTR response shows robust agonist-induced desensitization in multiple areas of the mouse brain. However, it cannot be excluded that this process is less pronounced or absent in a region of the brain that was not investigated in this study.

OXTR-induced spiking and presynaptic release responses undergo desensitization

There is immunohistochemical evidence for the localization of OXTR to the presynaptic active zone, postsynaptic density, and axon initial segment.[49] Furthermore, electrophysiological studies showed that OXTR activation causes varied effects in different neurons, which include postsynaptic transmission changes, spike generation, and presynaptic release modulation.[13–18,50] We inquired whether TGOT-induced spiking in LS neurons is derived from a cell autonomous effect on spike generation and/or caused by the presynaptic effect on neurotransmitter release. We further asked if the presynaptic and cell autonomous responses undergo similar desensitization. We first evaluated the cell autonomous effect of OXTR activation independent of presynaptic activity by recording spikes from OXTR LS neurons in the presence of an AMPA receptor blocker (NBQX, 20 μM) along with the $GABA_A$ receptor antagonist picrotoxin (50 μM). We found that spiking induced by sequential application of 200 nM TGOT showed robust acute desensitization and tachyphylaxis (Figure 2A). Similar results as earlier were obtained from sIPSC recordings on dorsal LS neurons in the presence of NBQX (Figure 2B). This indicates that OXTR activation can generate spiking in LS OXTR neurons independent of presynaptic activity, and this cell autonomous response undergoes robust agonist-induced desensitization. We next examined the contribution of presynaptic OXTR in the spiking of OXTR neurons in the LS. For this purpose, we recorded miniature excitatory postsynaptic currents (mEPSC) from OXTR neurons in the presence of tetrodotoxin (TTX 0.5 μM) to analyze a presynaptic effect of OXTR activation on glutamate release. We observed that TGOT (200 nM, 8 min) induced an increase in mEPSC frequency in only a minority of cells. Nevertheless, this mEPSC response underwent desensitization with no response to the second application of TGOT after 15 min washout (Figure 2C). These results show that both cell autonomous spike generation and presynaptic OXTR responses in the LS undergo desensitization.

OXTR desensitization in neurons occurs at the level of G protein activity

The desensitization of neuronal OXTR response could in principle arise due to agonist-induced inactivity of effector proteins (e.g., K^+ channels) or signaling mediators or due to G protein uncoupling from the receptor. To identify the underlying mechanisms, we used Bioluminescence Resonance Energy Transfer (BRET) assays in live cultured neurons. This technique is widely used to characterize ligand-dependent recruitment of intracellular proteins to GPCRs,[51,52] track receptors through cellular compartments,[53] and monitor cell signaling.[54,55] This method has been applied to OXTR expressed in heterologous cell lines[28,44] but the processes downstream of neuronal OXTR activation that become desensitized remained unknown. We first examined whether the immediate downstream signaling of OXTR, involving hydrolysis of $PI(4,5)P_2$ by phospholipase C-β (PLCβ), undergoes desensitization. For this purpose, we generated a probe for $PI(4,5)P_2$ hydrolysis consisting of two components expressed in lentiviral vectors (Figure 3A). This probe included (1) the energy donor nanoluciferase fused to the pleckstrin homology domain of PLCδ (nanoLuc−PH-PLCδ), which has the propensity to bind to $PI(4,5)P_2$,[56] and (2) the energy acceptor HaloTag fused to CAAX box, which targets it to the cell membrane[57] (Figure S5). We transduced primary neuronal cultures with these two lentiviral vectors along with lentivirus expressing mouse OXTR. Application of TGOT (200 nM) caused a strong immediate decrease in BRET ratio, indicating $PI(4,5)P_2$ hydrolysis and depletion, leading to the departure of nanoLuc−PH-PLCδ from the plasma membrane (Figure 3A). Importantly, the decrease reached a peak in the first few minutes and returned toward the baseline in the continued presence of the agonist. This indicates that agonist-induced desensitization following neuronal OXTR activation is present at the level of PLCβ function. The hydrolysis of $PI(4,5)P_2$ was downstream of $G\alpha_q$ because $G\alpha_q$ activity inhibitor UBO-QIC (1 μM) abolished the response but Gβγ inhibitor Gallein (40 μM) had no effect (Figures 3A and S4A). To further investigate if the abovementioned result is due to desensitization of PLCβ activity *per se* or arises due to upstream effect at the level of G proteins, we performed a BRET assay to analyze the time course of G protein activation in neurons. This assay monitors the release of Gβγ dimers from Gα upon receptor activation followed by their binding to GRK2/3.[58] We transduced primary neuronal cultures with lentivirus expressing nanoLuc-Gγ, Flag-Gβ, and GRK2-HaloTag. In response to TGOT (200 nM), we observed a rapid increase in the BRET ratio signifying G protein activation, but this ratio returned to baseline in the continued presence of the agonist indicating termination of G protein activation (Figure 3B). This result shows that desensitization of OXTR response in neurons arises at the level of G proteins, likely due to their inactivation or uncoupling from the receptor.

Agonist-dependent recruitment of β-arrestins and GRK2/3/6 to OXTR in neurons

The classical mechanism mediating G protein uncoupling from GPCRs is through competing binding of β-arrestins.[21,22,59]. In order to investigate if β-arrestin-1 and/or β-arrestin-2 are recruited to activated OXTR in neurons, we performed a BRET assay on primary neuronal cultures expressing OXTR-nanoLuc along with β-arrestin-1-HaloTag or β-arrestin-2-HaloTag (Figures 3C and S6). Application of TGOT (200 nM)

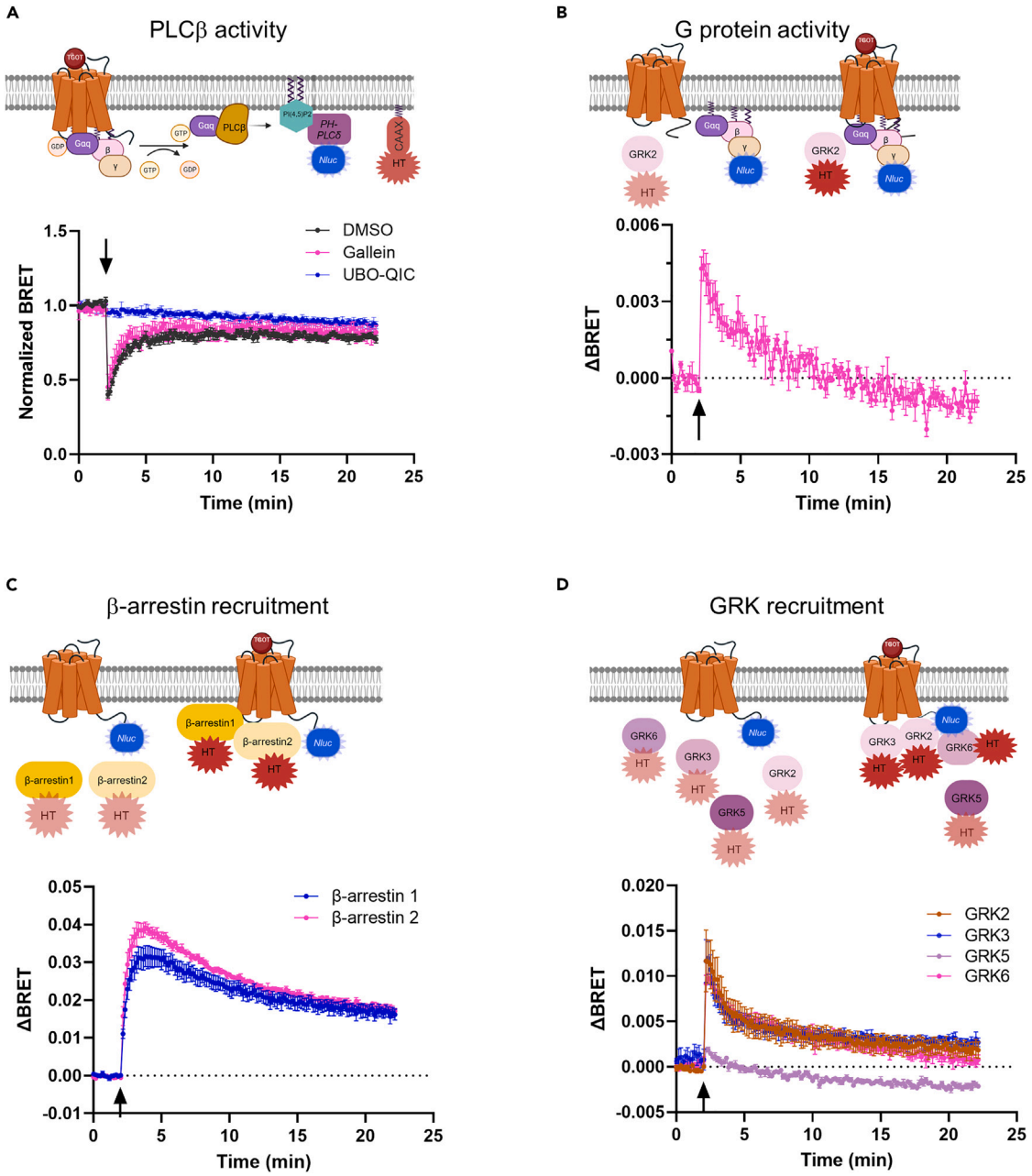

Figure 3. Desensitization of PI(4,5)P_2 hydrolysis and G protein activation, and recruitment of β-arrestin-1/2 and GRK2/3/6 to activated OXTR in primary neuronal cultures

(A) Summary graph (bottom) of normalized BRET showing the time course of PI(4,5)P_2 hydrolysis downstream of OXTR activation by 200 nM TGOT (time of application is indicated by an arrow). Schematic (top) shows the BRET configuration with nanoLuc-PH-PLCδ and HaloTag-CAAX. Normalized BRET is reduced rapidly with TGOT application in control (black) followed by quick recovery suggesting desensitization (n = 3). Gα_q inhibitor UBO-QIC (1 μM, blue) abolished the response, whereas Gβγ inhibitor Gallein (40 μM, magenta) had no effect (n = 3–5 per group).

(B) Summary graph (bottom) of ΔBRET showing the time course of G protein activation downstream of OXTR activation by 200 nM TGOT. Schematic (top) shows the BRET configuration with neurons expressing nanoLuc-Gγ, Gβ, and Gα_q along with GRK2-HaloTag. BRET is rapidly increased with TGOT application followed by quick recovery suggesting desensitization at the G protein level (n = 3).

(C) Summary graph (bottom) of ΔBRET showing the time course of recruitment of β-arrestin-1 and β-arrestin-2 to neuronal OXTR activated by 200 nM TGOT. Schematic (top) shows the BRET configuration with neurons expressing OXTR-nanoLuc and β-arrestin-1 (blue) or β-arrestin-2 (magenta). BRET is increased with TGOT application suggesting recruitment of both β-arrestins to neuronal OXTR (n = 3–5 per group).

Figure 3. *Continued*

(D) Summary graph (bottom) of ΔBRET time course shows that GRK2, GRK3, and GRK6 (but not GRK5) are recruited to neuronal OXTR activated by 200 nM TGOT. Schematic (top) shows the BRET configuration with neurons expressing OXTR-nanoLuc and GRK2-HaloTag (red), GRK3-HaloTag (blue), GRK5-HaloTag (gray), or GRK6-HaloTag (magenta) (n = 4 per group). The data in graphs are shown as mean ± SEM.

caused a gradual increase in BRET ratio with both β-arrestin-1-HaloTag and β-arrestin-2-HaloTag, indicating that both isoforms of β-arrestins are readily recruited to activated OXTR in neurons (Figure 3C). The BRET ratio peaked within 2–3 min and then decreased but persisted considerably above the baseline for the 20 min duration of recordings (Figures 3C, S4B, and S4C), suggesting long-lasting association of both β-arrestin isoforms to agonist-bound neuronal OXTR. The recruitment of β-arrestins is generally brought about by the phosphorylation of the receptor by GRK,[21–23,59] of which GRK2, GRK3, GRK5, and GRK6 are expressed in the brain (Figure S7). We investigated which isoforms of GRK are recruited to activated OXTR in neurons by performing a BRET assay on primary neuronal cultures expressing OXTR-nanoLuc along with GRK2, GRK3, GRK5, or GRK6, fused to HaloTag at their C-terminus (Figures 3D andS6). Application of TGOT (200 nM) led to a sharp rise in the BRET ratio with GRK2-HaloTag, GRK3-HaloTag, and GRK6-HaloTag, but not with GRK5-HaloTag (Figure 3D). The time course of recruitment of GRK isoforms was faster than that of β-arrestins, peaking in the first 10 s (Figures 3D and S4B). The association was also more time limited as the BRET ratio decreased rapidly to baseline after reaching the peak (Figures 3D and S4C). These findings identify the GRK isoforms that get recruited to activated OXTR in neurons and define the kinetics of their association.

β-arrestins are redundant while GRK2/3/6 are required for OXTR desensitization in neurons

To begin to decipher the molecular mechanisms that mediate desensitization of OXTR in neurons, we targeted β-arrestin-1 and -2 because they are readily recruited to agonist-bound neuronal OXTR as shown earlier and due to their reported involvement in OXTR desensitization in HEK293 cells and uterine myocytes.[28,29,33] We first obtained sIPSC recordings from dorsal LS neurons in constitutive β-arrestin-1 (*Arrb1*$^{-/-}$) knockout mice. Application of TGOT (200 nM, 1 min) showed robust increase in sIPSC frequency when applied the first time but elicited no significant response to the second application of TGOT after 15 min (Figures 4A and 4H). Similar results were obtained from the recordings in constitutive β-arrestin-2 (*Arrb2*$^{-/-}$) knockout mice (Figures 4B and 4H). These results show that OXTR desensitization in LS neurons is unaltered by the deletion of either of the two β-arrestin isoforms. Since there may be redundancy between the two isoforms, we developed a strategy based on CRISPR-Cas9 to obtain simultaneous deletion of the two isoforms in the LS. It is worth noting here that global deletion of *Arrb1* and *Arrb2* together is embryonically lethal.[60,61] We performed multigenerational crossing between *Arrb2*$^{-/-}$ and *Rosa26-LSL-Cas9*$^{Tg/Tg}$ mice to obtain *Arrb2*$^{-/-}$*;Rosa26-LSL-Cas9*$^{Tg/Tg}$ animals that were then stereotaxically injected in the LS with adeno-associated virus (AAV) expressing Cre and *Arrb1*-targeting gRNA (Figure 4C). Immunohistochemical staining of LS sections and immunoblots of LS lysates revealed robust depletion of β-arrestin-1 in the LS, thus obtaining efficient double knockout of the two β-arrestin isoforms in this brain region (Figures 4D and 4E). We proceeded to examine whether these molecular manipulations affect OXTR desensitization in LS neurons. Application of TGOT (200 nM, 1 min) elicited strong increase in sIPSC frequency in dorsal LS neurons when applied the first time but induced no significant response during the second application 15 min later, indicating robust desensitization (Figures 4F and 4H). These results unexpectedly show that β-arrestins are redundant for OXTR desensitization in mouse brain LS neurons.

GRKs can act independently of β-arrestins to mediate GPCR desensitization in addition to their prototypic role in promoting β-arrestin-dependent desensitization.[62–65] To examine the role of GRK2, GRK3, and GRK6 that were identified to be recruited to neuronal OXTR (Figure 3D), we utilized chemical inhibitors CMPD101 and GRK6-IN-2 (Compound 10a). These reagents inhibit the activity of GRK2/3 and GRK6, respectively, with high selectivity.[66,67] We preincubated acute brain slices from C57BL/6J mice with a mix of CMPD101 (50 μM) and GRK6-IN-2 (50 μM) for 30 min and then obtained sIPSC recordings from dorsal LS neurons in the continued presence of these inhibitors. Following the application of TGOT (200 nM, 1 min), we observed a strong increase in sIPSC frequency in dorsal LS neurons that persisted for a longer time than in control conditions (Figures 4G and S4D). In addition, we found a strong response to the second application of TGOT 15 min later, indicating suppression of desensitization (Figures 4G and 4H). These results show that GRK2/3/6 are required for OXTR desensitization in the mouse brain LS neurons.

Mechanisms underlying agonist-induced internalization of OXTR in neurons

An important process that contributes to the desensitization of most (but not all) GPCRs is the internalization of agonist-bound receptor that often leads to the termination of signaling.[62,68,69] It remained unexplored whether OXTR undergoes agonist-induced internalization in neurons, though there is evidence of this occurring in HEK293 cells.[30,31] To examine OXTR internalization in real time in live neurons, we adapted bystander BRET assays for application in primary neuronal cultures (Figure 5A). We tagged different compartments of membrane trafficking machinery by lentiviral expression of HaloTag fused to CAAX box (for plasma membrane), 2xFYVE domain (early endosome), and Rab11 (recycling endosome) (Figures S5 and S8).[53] We then performed BRET experiments on primary neurons expressing each of these constructs along with OXTR-nanoLuc. Application of TGOT (200 nM) led to an immediate decrease in BRET between OXTR-nanoLuc and HaloTag-CAAX that continued to grow over the 20 min of recording (Figure 5B). This shows robust internalization of activated OXTR in neurons. BRET between OXTR-nanoLuc and HaloTag-2xFYVE showed a TGOT-induced increase, indicating trafficking of internalized receptor to the early endosome (Figure 5B). Notably, this BRET ratio started increasing after a time lag of ~3 min from agonist application, defining the time it takes for the receptor to traffic from the cell membrane to early endosome in neurons. BRET between OXTR-nanoLuc and HaloTag-Rab11 also showed a TGOT-induced increase, indicating trafficking of receptors from early to recycling endosome, starting around

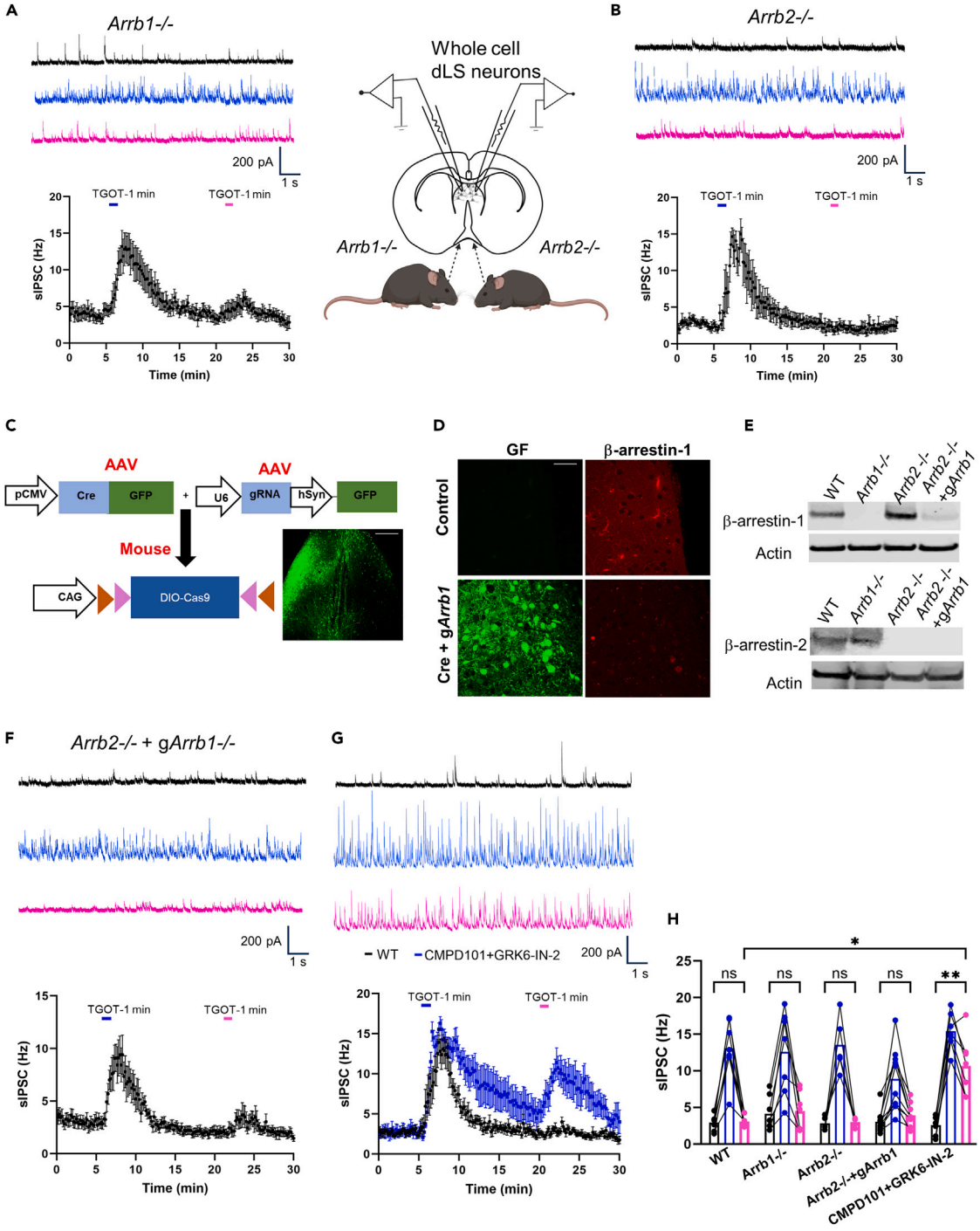

Figure 4. GRK2/3/6 are required while β-arrestins are redundant for neuronal OXTR desensitization

(A) Whole-cell recordings of sIPSC from dorsal LS neurons of β-arrestin-1 KO mice showing response to two applications of 200 nM TGOT for 1 min each separated by 15 min. Sample traces for baseline (black), first response (blue), and second response (magenta) (top) and summary graph of time course (bottom) are shown. The lack of robust second response compared to first indicates intact OXTR desensitization.

(B) Whole-cell recordings of sIPSC from dorsal LS neurons of β-arrestin-2 KO mice showing response to two applications of 200 nM TGOT for 1 min each separated by 15 min. Sample traces (top) and summary graph of time course (bottom) are shown. The lack of robust second response compared to first indicates intact OXTR desensitization.

(C) Schematic showing the strategy for CRISPR/Cas9-based KO of β-arrestin-1 in the LS of constitutive β-arrestin-2 KO mice. Inset shows expression of GFP from AAV GFP-Cre and AAV gRNA-Syn-GFP in the LS. Scale bar: 400 μm.

Figure 4. *Continued*

(D) Immunohistochemical confirmation of CRISPR/Cas9-induced depletion of β-arrestin-1 in the LS. Sections were stained with antibody against GFP or β-arrestin-1 in control and injected animals. Scale bar: 100 μm.

(E) Immunoblots on LS lysates from WT, β-arrestin-1 KO (*Arrb1*$^{-/-}$), β-arrestin-2 KO (*Arrb2*$^{-/-}$), and CRISPR/Cas9-induced β-arrestin-1 KO (*gArrb1*) in β-arrestin-2 KO mice. Blots were stained with antibodies against β-arrestin-1, β-arrestin-2, and β-actin.

(F) Whole-cell recordings of sIPSC from dorsal LS neurons of double β-arrestin KO mice showing response to two applications of 200 nM TGOT for 1 min each separated by 15 min. Sample traces (top) and summary graph of time course (bottom) are shown. The lack of robust second response compared to first indicates intact OXTR desensitization.

(G) Whole-cell recordings of sIPSC from dorsal LS neurons in control condition (brown) and in the presence of CMPD101 (50 μM) and GRK6-IN-2 (50 μM) (blue). The summary graph of the time course of response to two applications of 200 nM TGOT for 1 min each separated by 15 min is shown (bottom). There is strong response to the second TGOT application in the presence of CMPD101 and GRK6-IN-2, indicating suppression of OXTR desensitization. Sample traces for CMPD101+GRK6-IN-2 condition are shown above the graph.

(H) Bar graphs with baseline, first peak response, and second peak response in WT, β-arrestin-1 KO (*Arrb1*$^{-/-}$), β-arrestin-2 KO (*Arrb2*$^{-/-}$), double β-arrestin KO (*Arrb2*$^{-/-}$ + *gArrb1*), and GRK2/3/6 inhibition (CMPD101 + GRK6-IN-2). sIPSC frequency (Hz) WT: baseline, 2.920 ± 0.413; 1st response, 13.100 ± 1.538; 2nd response, 3.095 ± 0.314; n = 7 cells, 5 mice. sIPSC frequency (Hz) *Arrb1*$^{-/-}$: baseline, 4.136 ± 0.917; 1st response, 12.590 ± 2.155; 2nd response, 4.510 ± 1.003; n = 7 cells, 4 mice. sIPSC frequency (Hz) *Arrb2*$^{-/-}$: baseline, 2.813 ± 0.404; 1st response, 13.150 ± 1.410; 2nd response, 3.020 ± 0.277; n = 6 cells, 3 mice. sIPSC frequency (Hz) *Arrb2*$^{-/-}$ + *gArrb1*: baseline, 3.055 ± 0.486; 1st response, 8.880 ± 1.342; 2nd response, 3.927 ± 0.468; n = 10 cells, 6 mice. sIPSC frequency (Hz) CMPD101 + GRK6-IN-2: baseline, 2.600 ± 0.491; 1st response, 15.410 ± 0.946; 2nd response, 10.680 ± 1.506; n = 7 cells, 5 mice. The data in graphs are shown as mean ± SEM. **p < 0.01, ***p < 0.001, ****p < 0.0001, Repeated measures two-way ANOVA with post-hoc Tukey's multiple comparisons test.

~6 min post-application (Figure 5B). We then investigated the molecular mechanism and membrane compartment/s mediating the trafficking of neuronal OXTR from the cell membrane to early endosome. For this purpose, we assayed BRET with Rab5 and Rab21 fused to HaloTag (Figure S8) as these GTPases have been shown to mark alternative routes to early endosomes for specific membrane proteins.[70] TGOT application (200 nM) caused an increase in BRET from OXTR-nanoLuc to HaloTag-Rab5 but not to HaloTag-Rab21 (Figure 5C), which indicates that neuronal OXTR traffics to early endosome through a Rab5-labeled compartment. To confirm the role of Rab5 in trafficking, we expressed a dominant negative mutant of Rab5, Rab5 S34N (Rab5 DN) in neurons.[71,72] TGOT-induced increase in BRET between OXTR-nanoLuc and HaloTag-2xFYVE was abolished by Rab5 DN (Figure 5D), providing further evidence of the role of Rab5 in mediating trafficking of neuronal OXTR from cell membrane to early endosome. Notably, dominant negative Rab5 did not alter TGOT-induced decrease in BRET between OXTR-nanoLuc and HaloTag-CAAX (Figure 5E), which along with previous result suggests that OXTR are still internalized in the absence of Rab5 activity but fail to reach their regular destination in early endosome.

We next investigated whether β-arrestins and GRKs are involved in neuronal OXTR internalization to complement our results on desensitization in LS slices. Preincubation of neuronal cultures with GRK2/3 inhibitor CMPD101 (50 μM) did not alter the TGOT-induced decrease in BRET between OXTR-nanoLuc and HaloTag-CAAX (Figure 5F). Similar results were obtained in the presence of GRK6 inhibitors GRK6-IN-1/Compound 18 (50 μM) and GRK6-IN-2 (50 μM).[67] However, the application of CMPD101 along with GRK-6-IN-1 or GRK-6-IN-2 abolished the agonist-induced decrease in BRET between OXTR-nanoLuc and HaloTag-CAAX (Figures 5F and S9). In contrast, preincubation with Barbadin (100 μM), which inhibits β-arrestin-dependent endocytosis by interfering with β-arrestin-AP2 interaction,[73–75] had no effect. These results show that GRK2/3/6 are involved in inducing agonist-dependent OXTR internalization in neurons and indicate that these isoforms are individually redundant in this process. Furthermore, β-arrestins do not appear to be involved in neuronal OXTR internalization. These results complement our results on the requirement of GRK2/3/6 and redundancy of β-arrestins in OXTR desensitization in mouse brain slices.

DISCUSSION

The present study identifies robust agonist-induced desensitization and internalization of OXTR in mouse brain neurons and elucidates the underlying molecular mechanisms. We find that many molecular properties differ from what has been reported in studies on OXTR in heterologous cells and uterine myometrial cells. This is in line with the increasing realization that GPCRs are regulated differently in their native environment compared to when they are expressed in cell lines and that the mechanisms may even differ between different native tissues and cells. By identifying the molecular mechanisms that mediate OXTR desensitization in neurons, our results provide novel information on the intracellular regulation of this GPCR in the brain that has implications for understanding its role in social and other affective behavior.

Using electrophysiology assays in *ex vivo* brain slices, we found robust agonist-induced desensitization in multiple regions of the mouse brain that included the LS, PFC, and BNST. Our use of TGOT as the agonist in most experiments ensured that the responses were elicited selectively from OXTR, as TGOT unlike oxytocin does not activate rodent vasopressin receptors such as AVPR1a that are expressed heavily in the examined brain regions.[43,45] Nevertheless, we confirmed robust desensitization in response to the endogenous agonist oxytocin applied in the presence of AVPR1a antagonists. Previously published work on rat brain reported region-specific differences in desensitization of oxytocin-induced response, with some regions showing little desensitization.[34,35] This discrepancy with our work may be due to species-specific differences or because of off-target activation (and possible lack of desensitization) of vasopressin receptors by bath-applied oxytocin in the rat studies.

Even though BRET has been extensively used in the GPCR field, its application to studies in neurons has been very limited. Our study constitutes one of the first systematic application of BRET assays in neuronal cultures to analyze various aspects of GPCR biology including G protein activation, PI(4,5)P_2 hydrolysis, β-arrestin and GRK recruitment, and receptor trafficking. The results obtained from PI(4,5)P_2 hydrolysis

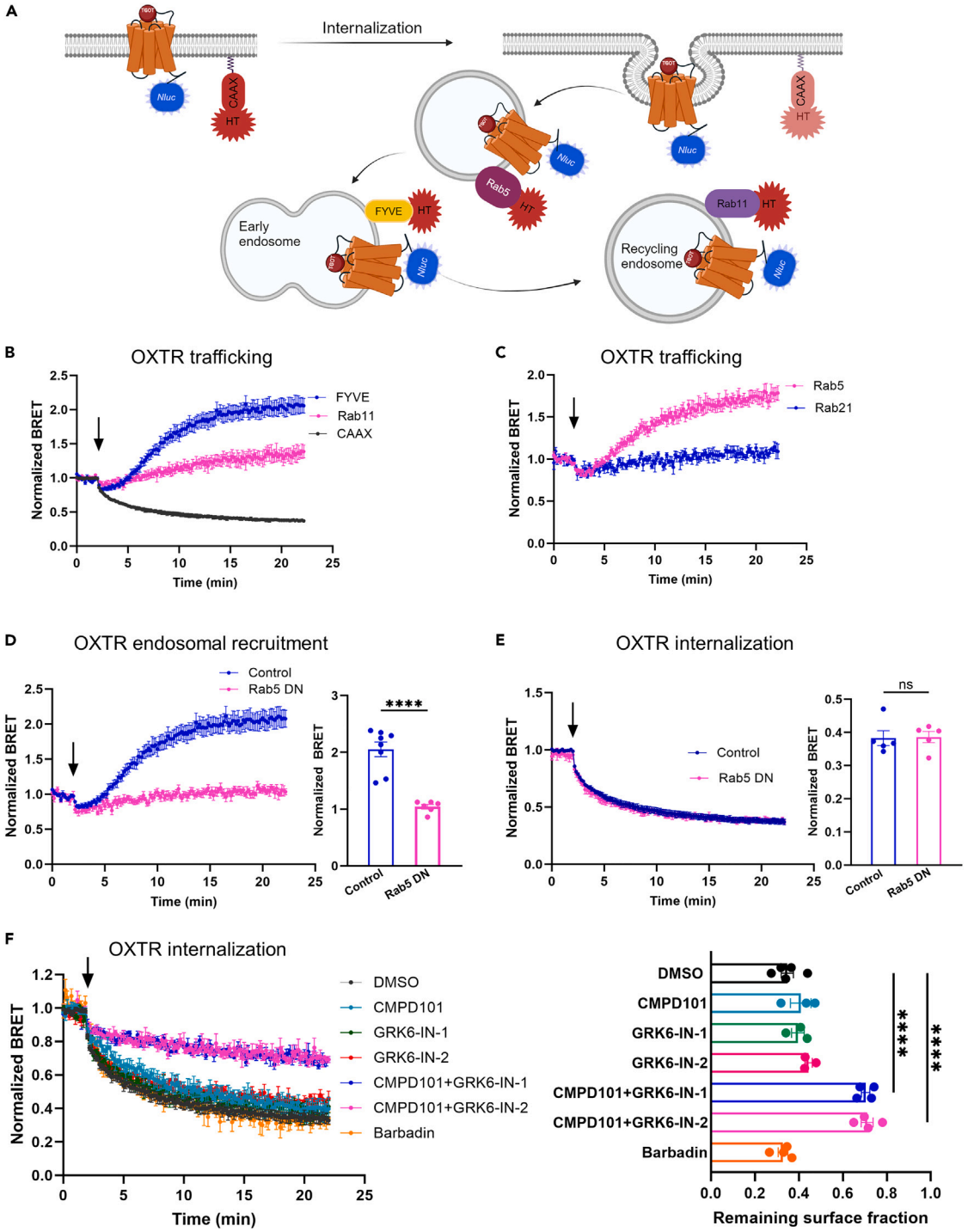

Figure 5. Molecular mechanisms underlying agonist-induced internalization and trafficking of neuronal OXTR

(A) Schematic depicting BRET assays for tracking OXTR internalization and trafficking in primary neuronal cultures. BRET was configured with OXTR-nanoLuc along with HaloTag-CAAX (for cell membrane localization), HaloTag-2xFYVE (early endosome), HaloTag-Rab11 (recycling endosome), HaloTag-Rab5 (Rab5 compartment), and HaloTag-Rab21 (Rab21 compartment).

(B) Summary graph of normalized BRET showing the time course of neuronal OXTR internalization (HaloTag-CAAX), trafficking to early endosomes (HaloTag-2xFYVE) and moving into recycling endosomes (HaloTag-Rab11) following application of 200 nM TGOT (time of application is indicated by an arrow) (n = 3–9 per group).

Figure 5. *Continued*

(C) Summary graph of normalized BRET showing the time course of neuronal OXTR trafficking to Rab5-but not Rab21-containing endosomes following application of 200 nM TGOT (n = 3–5 per group).

(D) Trafficking of neuronal OXTR to early endosomes in response to 200 nM TGOT was impaired with expression of dominant negative Rab5 (Rab5 DN). Summary graph of the time course (left) of normalized BRET with OXTR-nanoLuc and HaloTag-2xFYVE. The bar graph of the averaged normalized BRET response for the last 5 min is shown on right. Control, 2.052 ± 0.128; Rab5 DN, 1.043 ± 0.041; n = 6–8 per group.

(E) Internalization of neuronal OXTR in response to 200 nM TGOT was not affected with expression of dominant negative Rab5 (Rab5 DN). Summary graph of the time course (left) of normalized BRET with OXTR-nanoLuc and HaloTag-CAAX is shown. The bar graph of the averaged normalized BRET response for the last 5 min is shown on right. Control, 0.383 ± 0.023; Rab5 DN, 0.386 ± 0.017; n = 5 per group.

(F) Summary graph (left) of normalized BRET showing the time course of neuronal OXTR internalization in the presence of vehicle (DMSO), Barbadin, CMPD101, GRK6-IN-1, GRK6-IN-2, and a mix of CMPD101 and GRK6-IN-1 (CMPD101+GRK6-IN-1) or a mix of CMPD101 and GRK6-IN-2 (CMPD101+GRK6-IN-2). BRET was configured with OXTR-nanoLuc and HaloTag-CAAX. The internalization was impaired in the presence of a mix of CMPD101 and GRK6-IN-2 but not with Barbadin, CMPD101, or GRK6-IN-2 alone. The bar graph of the averaged normalized BRET response for the last 5 min is shown on right. DMSO, 0.348 ± 0.027; CMPD101, 0.409 ± 0.046; GRK6-IN-1, 0.396 ± 0.029; GRK6-IN-2, 0.445 ± 0.017; CMPD101 + GRK6-IN-1, 0.703 ± 0.019; CMPD101 +GRK6-IN-2, 0.711 ± 0.027; Barbadin, 0.328 ± 0.022; n = 3–5 per group. The data in graphs are shown as mean ± SEM. ****$p < 0.0001$, unpaired Student's t test (D and E) or one-way ANOVA with post-hoc Dunnett's test (F).

BRET assay show that neuronal OXTR activation induces $PI(4,5)P_2$ hydrolysis in a $G\alpha_q$-dependent manner, confirming coupling of neuronal OXTR to $G\alpha_q$ pathway. The lack of effect of Gallein in this assay suggests that the reported role of $G\beta\gamma$ in activating PLCβ[76,77] does not apply to neuronal OXTR. This may not be surprising considering that $G\beta\gamma$, downstream of $G\alpha_{i/o}$ but not $G\alpha_q$, activates PLCβ.[76,77] However, OXTR has been shown to couple to $G\alpha_{i/o}$ in addition to its primary association with $G\alpha_q$.[78] Our result with Gallein thus show that this pathway is not responsible for PLCβ activation downstream of OXTR in neurons. Importantly, the time courses of $PI(4,5)P_2$ hydrolysis and free $G\beta\gamma$ (in the GRK-Gγ assay) in the continued presence of the ligand reveal that desensitization of OXTR response in neurons occurs at the level of G protein activation on the receptor, upstream of any desensitization of effector proteins such as potassium channels. The similarity of time courses in the two assays also suggests that depletion of $PI(4,5)P_2$ is normally not a rate-limiting factor downstream of neuronal OXTR, as membrane $PI(4,5)P_2$ levels are restored as soon as G proteins get inactivated (reflected in decay of free $G\beta\gamma$). This is likely due to ample amounts of $PI(4,5)P_2$ present in the neuronal membrane or its quick regeneration.

Our BRET experiments show robust agonist-induced internalization of OXTR in neurons and their subsequent trafficking to early and recycling endosomes. The time course of internalization appears similar to results obtained from immunocytochemical studies in heterologous cells,[30,31] though the real-time analysis provided by BRET accurately reveals the temporal delay in movement between compartments in neurons. The delay of ~3 min in the transfer from CAAX-decorated cell membrane to early endosome is likely due to time spent routing through endocytic vesicles and/or CAAX-negative membrane microdomains. The results also clarify that neuronal OXTR traffics through a Rab5 compartment and that Rab5 is required for the trafficking of neuronal OXTR to early endosomes. The former finding aligns with data obtained in HEK293 cells internalization[30] but the requirement of Rab5 for OXTR entry into early endosomes was not tested in previous studies. Notably, the trafficking of OXTR to Rab11-containing recycling endosomes (starting ~6 min after agonist binding) appears to be unique to neurons as it was not observed previously in HEK293 cells and uterine myocytes.[30]

OXTR has been shown to have a stable association with β-arrestins in heterologous cells following agonist binding.[31] Our BRET results in neurons agree with this finding in general but show a more substantial decrease in association over time in the continued presence of the agonist compared to HEK293 cells. This could be due to weaker interaction between OXTR and β-arrestin-1 and -2 in neurons (see later discussion). Importantly, we found that β-arrestins are not required for OXTR desensitization or internalization in neurons. This result is surprising because there is efficient recruitment of β-arrestin-1 and -2 to neuronal OXTR and previous work provided evidence for their requirement in OXTR desensitization and internalization in HEK293 cells and uterine myocytes.[29,33] The evidence though from previous work has limitations. The study in HEK293 cells did not use a knockdown or knockout approach but utilized the expression of a dominant negative mutant of arrestin to find a modest (<25%) reduction in internalization and somewhat larger decrease in desensitization of OXTR response.[29] Brighton et al. reported that knockdown of β-arrestin-1 or -2 in uterine myocytes reduced desensitization by only half, whereas simultaneous deletion of both isoforms was not attempted.[33] Nevertheless, our results from neurons show that OXTR desensitization and internalization are not altered following genetic deletion of both β-arrestins or pharmacological inhibition of β-arrestin-AP2 interaction. The mechanism underlying these cell-specific differences would need to be deciphered. The presence of a second parallel mechanism in neurons may make the β-arrestins redundant for neuronal OXTR desensitization despite their involvement. Alternatively, β-arrestins may bind only to the C-terminal tail of neuronal OXTR and not to the core (formed by intracellular loops), which may be sufficient to initiate signaling pathways but not the dislodgement of G proteins required for desensitization.

A major finding of this study is that GRK2, GRK3, and GRK6 are the GRK isoforms that are recruited to OXTR in neurons and are individually redundant but together required for the desensitization and internalization. This is a surprising finding because previous studies found only one GRK isoform to mediate OXTR desensitization in HEK293 cells (GRK2) and uterine myometrium (GRK6).[29,32] The redundancy among the three GRK isoforms along with redundancy of β-arrestins suggest a richness of mechanisms that are involved in desensitization of OXTR and likely other GPCRs in neurons. How do GRK2/3/6 mediate neuronal OXTR desensitization and internalization? The use of kinase activity blockers in our experiments provides unambiguous evidence that GRKs orchestrate this by phosphorylating downstream targets. This is an important conclusion because evidence exists for some GPCRs for an alternative β-arrestin-independent pathway via direct binding of

GRK to Gα, independent of kinase activity.[62–64] In terms of GRK targets, our results clearly show that neuronal OXTR is phosphorylated by GRK2/3/6 as β-arrestins (that recognize phosphorylated sequences) are readily recruited to the receptor and this binding is disrupted with GRK2/3/6 inhibitors. Future experiments involving identification of GRK phosphorylation sites within OXTR and molecular replacement with phospho-null mutants will further clarify the mechanism by which GRK-induced phosphorylation mediates OXTR desensitization and internalization in neurons.

The understanding of the desensitization mechanisms will allow us to elucidate the physiological significance of this process in oxytocin-dependent animal behavior. The decremental social preference over time seen in some behavioral assays[79] may be mediated by OXTR desensitization, thus manipulating the underlying mechanisms may result in improved social scores. Future effort will also need to be directed to investigate if ASD-associated OXTR variants show altered desensitization that results in detrimental effects on social and other affective behavior.

Limitations of the study

We have used TGOT to selectively activate OXTR in most experiments reported in this study. Although we demonstrate that neuronal responses undergo similar desensitization upon exposure to the native neuropeptide oxytocin and TGOT, it is possible that the underlying mechanisms may differ between the two agonists. It is also uncertain what concentrations of oxytocin are obtained in the vicinity of OXTR at specific brain regions during behavior and whether they provoke comparable desensitization responses. We have not investigated the offset kinetics of the desensitization process, because the patch-clamp recording in brain slices require that we complete the experiment within an hour or so, which limits the length of the interval between the two agonist applications. Our conclusions on the molecular mechanisms underlying neuronal OXTR desensitization are derived principally from *ex vivo* studies in the LS (which has exclusive GABAergic neurons), and it remains possible that mechanisms in other brain regions or neuronal sub-types are different. The cultured cortical neurons do not consistently express OXTR, thus this system may not perfectly recapitulate the native neuronal environment. However, the complementary results obtained from *ex vivo* brain slices of the LS and primary neuronal cultures in our study strengthen the validity of our approach.

STAR★METHODS

Detailed methods are provided in the online version of this paper and include the following:

- KEY RESOURCES TABLE
- RESOURCE AVAILABILITY
  - Lead contact
  - Materials availability
  - Data and code availability
- EXPERIMENTAL MODEL AND STUDY PARTICIPANT DETAILS
- METHOD DETAILS
  - Plasmids and viral vectors
  - Stereotaxic surgery
  - Electrophysiological recordings
  - Immunohistochemistry and immunoblotting
  - Primary neuronal cultures
  - Bioluminescence Resonance Energy Transfer (BRET)
  - Drugs
- QUANTIFICATION AND STATISTICAL ANALYSIS

SUPPLEMENTAL INFORMATION

Supplemental information can be found online at https://doi.org/10.1016/j.isci.2024.110047.

ACKNOWLEDGMENTS

This study was supported by the NIMH/NIH grant R01MH125998 (M.A.), Whitehall Foundation grant 2021-08-077 (M.A.), and a Presbyterian Health Foundation grant (M.A.). The content is solely the responsibility of the authors and does not necessarily represent the official views of the National Institutes of Health. We thank Drs. Leonidas Tsiokas, Augen Pioszak, and Martin-Paul Agbaga for useful discussions and advice and Dr. Lori Garman for help with statistical analyses. We also thank the Cell Biology Imaging Core for access to the confocal microscope and the OUHSC Animal Research Facility for animal husbandry.

AUTHOR CONTRIBUTIONS

K.G., H.T.M.H., T.T., R.Y.N., and E.T.-R. performed experiments and analyzed data. G.L. provided reagents. M.A. supervised and acquired funding. K.G. and H.T.M.H. prepared the figures. M.A. wrote the paper.

DECLARATION OF INTERESTS

The authors declare no competing interests.

Received: November 6, 2023
Revised: February 22, 2024
Accepted: May 17, 2024
Published: May 22, 2024

REFERENCES

1. Gimpl, G., and Fahrenholz, F. (2001). The oxytocin receptor system: structure, function, and regulation. Physiol. Rev. *81*, 629–683. https://doi.org/10.1152/physrev.2001.81.2.629.
2. Menon, R., and Neumann, I.D. (2023). Detection, processing and reinforcement of social cues: regulation by the oxytocin system. Nat. Rev. Neurosci. *24*, 761–777. https://doi.org/10.1038/s41583-023-00759-w.
3. Neumann, I.D., and Slattery, D.A. (2016). Oxytocin in General Anxiety and Social Fear: A Translational Approach. Biol. Psychiatry *79*, 213–221. https://doi.org/10.1016/j.biopsych.2015.06.004.
4. Jurek, B., and Neumann, I.D. (2018). The Oxytocin Receptor: From Intracellular Signaling to Behavior. Physiol. Rev. *98*, 1805–1908. https://doi.org/10.1152/physrev.00031.2017.
5. Elagoz Yuksel, M., Yuceturk, B., Karatas, O.F., Ozen, M., and Dogangun, B. (2016). The altered promoter methylation of oxytocin receptor gene in autism. J. Neurogenet. *30*, 280–284. https://doi.org/10.1080/01677063.2016.1202951.
6. LoParo, D., and Waldman, I.D. (2015). The oxytocin receptor gene (OXTR) is associated with autism spectrum disorder: a meta-analysis. Mol. Psychiatry *20*, 640–646. https://doi.org/10.1038/mp.2014.77.
7. Ma, W.J., Hashii, M., Munesue, T., Hayashi, K., Yagi, K., Yamagishi, M., Higashida, H., and Yokoyama, S. (2013). Non-synonymous single-nucleotide variations of the human oxytocin receptor gene and autism spectrum disorders: a case-control study in a Japanese population and functional analysis. Mol. Autism. *4*, 22. https://doi.org/10.1186/2040-2392-4-22.
8. Lee, H.J., Caldwell, H.K., Macbeth, A.H., Tolu, S.G., and Young, W.S., 3rd (2008). A conditional knockout mouse line of the oxytocin receptor. Endocrinology *149*, 3256–3263. https://doi.org/10.1210/en.2007-1710.
9. Leonzino, M., Ponzoni, L., Braida, D., Gigliucci, V., Busnelli, M., Ceresini, I., Duque-Wilckens, N., Nishimori, K., Trainor, B.C., Sala, M., and Chini, B. (2019). Impaired approach to novelty and striatal alterations in the oxytocin receptor deficient mouse model of autism. Horm. Behav. *114*, 104543. https://doi.org/10.1016/j.yhbeh.2019.06.007.
10. Pobbe, R.L.H., Pearson, B.L., Defensor, E.B., Bolivar, V.J., Young, W.S., 3rd, Lee, H.J., Blanchard, D.C., and Blanchard, R.J. (2012). Oxytocin receptor knockout mice display deficits in the expression of autism-related behaviors. Horm. Behav. *61*, 436–444. https://doi.org/10.1016/j.yhbeh.2011.10.010.
11. Sala, M., Braida, D., Donzelli, A., Martucci, R., Busnelli, M., Bulgheroni, E., Rubino, T., Parolaro, D., Nishimori, K., and Chini, B. (2013). Mice heterozygous for the oxytocin receptor gene (Oxtr(+/-)) show impaired social behaviour but not increased aggression or cognitive inflexibility: evidence of a selective haploinsufficiency gene effect. J. Neuroendocrinol. *25*, 107–118. https://doi.org/10.1111/j.1365-2826.2012.02385.x.
12. Takayanagi, Y., Yoshida, M., Bielsky, I.F., Ross, H.E., Kawamata, M., Onaka, T., Yanagisawa, T., Kimura, T., Matzuk, M.M., Young, L.J., and Nishimori, K. (2005). Pervasive social deficits, but normal parturition, in oxytocin receptor-deficient mice. Proc. Natl. Acad. Sci. USA *102*, 16096–16101. https://doi.org/10.1073/pnas.0505312102.
13. Owen, S.F., Tuncdemir, S.N., Bader, P.L., Tirko, N.N., Fishell, G., and Tsien, R.W. (2013). Oxytocin enhances hippocampal spike transmission by modulating fast-spiking interneurons. Nature *500*, 458–462. https://doi.org/10.1038/nature12330.
14. Tirko, N.N., Eyring, K.W., Carcea, I., Mitre, M., Chao, M.V., Froemke, R.C., and Tsien, R.W. (2018). Oxytocin Transforms Firing Mode of CA2 Hippocampal Neurons. Neuron *100*, 593–608.e3. https://doi.org/10.1016/j.neuron.2018.09.008.
15. Dolen, G., Darvishzadeh, A., Huang, K.W., and Malenka, R.C. (2013). Social reward requires coordinated activity of nucleus accumbens oxytocin and serotonin. Nature *501*, 179–184. https://doi.org/10.1038/nature12518.
16. Hung, L.W., Neuner, S., Polepalli, J.S., Beier, K.T., Wright, M., Walsh, J.J., Lewis, E.M., Luo, L., Deisseroth, K., Dölen, G., and Malenka, R.C. (2017). Gating of social reward by oxytocin in the ventral tegmental area. Science *357*, 1406–1411. https://doi.org/10.1126/science.aan4994.
17. Ninan, I. (2011). Oxytocin suppresses basal glutamatergic transmission but facilitates activity-dependent synaptic potentiation in the medial prefrontal cortex. J. Neurochem. *119*, 324–331. https://doi.org/10.1111/j.1471-4159.2011.07430.x.
18. Huber, D., Veinante, P., and Stoop, R. (2005). Vasopressin and oxytocin excite distinct neuronal populations in the central amygdala. Science *308*, 245–248. https://doi.org/10.1126/science.1105636.
19. Kelly, E., Bailey, C.P., and Henderson, G. (2008). Agonist-selective mechanisms of GPCR desensitization. Br. J. Pharmacol. *153*, S379–S388. https://doi.org/10.1038/sj.bjp.0707604.
20. Rajagopal, S., and Shenoy, S.K. (2018). GPCR desensitization: Acute and prolonged phases. Cell. Signal. *41*, 9–16. https://doi.org/10.1016/j.cellsig.2017.01.024.
21. Gainetdinov, R.R., Premont, R.T., Bohn, L.M., Lefkowitz, R.J., and Caron, M.G. (2004). Desensitization of G protein-coupled receptors and neuronal functions. Annu. Rev. Neurosci. *27*, 107–144. https://doi.org/10.1146/annurev.neuro.27.070203.144206.
22. Luttrell, L.M., and Lefkowitz, R.J. (2002). The role of beta-arrestins in the termination and transduction of G-protein-coupled receptor signals. J. Cell Sci. *115*, 455–465.
23. Moore, C.A.C., Milano, S.K., and Benovic, J.L. (2007). Regulation of receptor trafficking by GRKs and arrestins. Annu. Rev. Physiol. *69*, 451–482. https://doi.org/10.1146/annurev.physiol.69.022405.154712.
24. Blanchet, C., and Lüscher, C. (2002). Desensitization of mu-opioid receptor-evoked potassium currents: initiation at the receptor, expression at the effector. Proc. Natl. Acad. Sci. USA *99*, 4674–4679. https://doi.org/10.1073/pnas.072075399.
25. Turecek, R., Schwenk, J., Fritzius, T., Ivankova, K., Zolles, G., Adelfinger, L., Jacquier, V., Besseyrias, V., Gassmann, M., Schulte, U., et al. (2014). Auxiliary GABAB receptor subunits uncouple G protein βγ subunits from effector channels to induce desensitization. Neuron *82*, 1032–1044. https://doi.org/10.1016/j.neuron.2014.04.015.
26. Tobin, A.B., Butcher, A.J., and Kong, K.C. (2008). Location, location, location...site-specific GPCR phosphorylation offers a mechanism for cell-type-specific signalling. Trends Pharmacol. Sci. *29*, 413–420. https://doi.org/10.1016/j.tips.2008.05.006.
27. Ritter, S.L., and Hall, R.A. (2009). Fine-tuning of GPCR activity by receptor-interacting proteins. Nat. Rev. Mol. Cell Biol. *10*, 819–830. https://doi.org/10.1038/nrm2803.
28. Hasbi, A., Devost, D., Laporte, S.A., and Zingg, H.H. (2004). Real-time detection of interactions between the human oxytocin receptor and G protein-coupled receptor kinase-2. Mol. Endocrinol. *18*, 1277–1286. https://doi.org/10.1210/me.2003-0440.
29. Smith, M.P., Ayad, V.J., Mundell, S.J., McArdle, C.A., Kelly, E., and López Bernal, A. (2006). Internalization and desensitization of the oxytocin receptor is inhibited by Dynamin and clathrin mutants in human embryonic kidney 293 cells. Mol. Endocrinol. *20*, 379–388. https://doi.org/10.1210/me.2005-0031.
30. Conti, F., Sertic, S., Reversi, A., and Chini, B. (2009). Intracellular trafficking of the human oxytocin receptor: evidence of receptor recycling via a Rab4/Rab5 "short cycle. Am. J. Physiol. Endocrinol. Metab. *296*, E532–E542. https://doi.org/10.1152/ajpendo.90590.2008.
31. Oakley, R.H., Laporte, S.A., Holt, J.A., Barak, L.S., and Caron, M.G. (2001). Molecular determinants underlying the formation of stable intracellular G protein-coupled receptor-beta-arrestin complexes after receptor endocytosis. J. Biol. Chem. *276*, 19452–19460. https://doi.org/10.1074/jbc.M101450200.
32. Willets, J.M., Brighton, P.J., Mistry, R., Morris, G.E., Konje, J.C., and Challiss, R.A.J. (2009).

Regulation of oxytocin receptor responsiveness by G protein-coupled receptor kinase 6 in human myometrial smooth muscle. Mol. Endocrinol. *23*, 1272–1280. https://doi.org/10.1210/me.2009-0047.
33. Brighton, P.J., Rana, S., Challiss, R.J., Konje, J.C., and Willets, J.M. (2011). Arrestins differentially regulate histamine- and oxytocin-evoked phospholipase C and mitogen-activated protein kinase signalling in myometrial cells. Br. J. Pharmacol. *162*, 1603–1617. https://doi.org/10.1111/j.1476-5381.2010.01173.x.
34. Terenzi, M.G., and Ingram, C.D. (2005). Oxytocin-induced excitation of neurones in the rat central and medial amygdaloid nuclei. Neuroscience *134*, 345–354. https://doi.org/10.1016/j.neuroscience.2005.04.004.
35. Wilson, B.C., Terenzi, M.G., and Ingram, C.D. (2005). Differential excitatory responses to oxytocin in sub-divisions of the bed nuclei of the stria terminalis. Neuropeptides *39*, 403–407. https://doi.org/10.1016/j.npep.2005.04.001.
36. Horiai, M., Otsuka, A., Hidema, S., Hiraoka, Y., Hayashi, R., Miyazaki, S., Furuse, T., Mizukami, H., Teruyama, R., Tamura, M., et al. (2020). Targeting oxytocin receptor (Oxtr)-expressing neurons in the lateral septum to restore social novelty in autism spectrum disorder mouse models. Sci. Rep. *10*, 22173. https://doi.org/10.1038/s41598-020-79109-0.
37. Son, S., Manjila, S.B., Newmaster, K.T., Wu, Y.T., Vanselow, D.J., Ciarletta, M., Anthony, T.E., Cheng, K.C., and Kim, Y. (2022). Whole-Brain Wiring Diagram of Oxytocin System in Adult Mice. J. Neurosci. *42*, 5021–5033. https://doi.org/10.1523/JNEUROSCI.0307-22.2022.
38. Newmaster, K.T., Nolan, Z.T., Chon, U., Vanselow, D.J., Weit, A.R., Tabbaa, M., Hidema, S., Nishimori, K., Hammock, E.A.D., and Kim, Y. (2020). Quantitative cellular-resolution map of the oxytocin receptor in postnatally developing mouse brains. Nat. Commun. *11*, 1885. https://doi.org/10.1038/s41467-020-15659-1.
39. Guzman, Y.F., Tronson, N.C., Sato, K., Mesic, I., Guedea, A.L., Nishimori, K., and Radulovic, J. (2014). Role of oxytocin receptors in modulation of fear by social memory. Psychopharmacology (Berl) *231*, 2097–2105. https://doi.org/10.1007/s00213-013-3356-6.
40. Mesic, I., Guzman, Y.F., Guedea, A.L., Jovasevic, V., Corcoran, K.A., Leaderbrand, K., Nishimori, K., Contractor, A., and Radulovic, J. (2015). Double Dissociation of the Roles of Metabotropic Glutamate Receptor 5 and Oxytocin Receptor in Discrete Social Behaviors. Neuropsychopharmacology *40*, 2337–2346. https://doi.org/10.1038/npp.2015.81.
41. Menon, R., Grund, T., Zoicas, I., Althammer, F., Fiedler, D., Biermeier, V., Bosch, O.J., Hiraoka, Y., Nishimori, K., Eliava, M., et al. (2018). Oxytocin Signaling in the Lateral Septum Prevents Social Fear during Lactation. Curr. Biol. *28*, 1066–1078.e6. https://doi.org/10.1016/j.cub.2018.02.044.
42. Zoicas, I., Slattery, D.A., and Neumann, I.D. (2014). Brain oxytocin in social fear conditioning and its extinction: involvement of the lateral septum. Neuropsychopharmacology *39*, 3027–3035. https://doi.org/10.1038/npp.2014.156.
43. Oliveira, V.E.d.M., Lukas, M., Wolf, H.N., Durante, E., Lorenz, A., Mayer, A.L., Bludau, A., Bosch, O.J., Grinevich, V., Egger, V., et al. (2021). Oxytocin and vasopressin within the ventral and dorsal lateral septum modulate aggression in female rats. Nat. Commun. *12*, 2900. https://doi.org/10.1038/s41467-021-23064-5.
44. Busnelli, M., Bulgheroni, E., Manning, M., Kleinau, G., and Chini, B. (2013). Selective and potent agonists and antagonists for investigating the role of mouse oxytocin receptors. J. Pharmacol. Exp. Ther. *346*, 318–327. https://doi.org/10.1124/jpet.113.202994.
45. Allaman-Exertier, G., Reymond-Marron, I., Tribollet, E., and Raggenbass, M. (2007). Vasopressin modulates lateral septal network activity via two distinct electrophysiological mechanisms. Eur. J. Neurosci. *26*, 2633–2642. https://doi.org/10.1111/j.1460-9568.2007.05866.x.
46. Song, Z., and Albers, H.E. (2018). Cross-talk among oxytocin and arginine-vasopressin receptors: Relevance for basic and clinical studies of the brain and periphery. Front. Neuroendocrinol. *51*, 14–24. https://doi.org/10.1016/j.yfrne.2017.10.004.
47. Tan, Y., Singhal, S.M., Harden, S.W., Cahill, K.M., Nguyen, D.T.M., Colon-Perez, L.M., Sahagian, T.J., Thinschmidt, J.S., de Kloet, A.D., Febo, M., et al. (2019). Oxytocin Receptors Are Expressed by Glutamatergic Prefrontal Cortical Neurons That Selectively Modulate Social Recognition. J. Neurosci. *39*, 3249–3263. https://doi.org/10.1523/JNEUROSCI.2944-18.2019.
48. Nakajima, M., Görlich, A., and Heintz, N. (2014). Oxytocin modulates female sociosexual behavior through a specific class of prefrontal cortical interneurons. Cell *159*, 295–305. https://doi.org/10.1016/j.cell.2014.09.020.
49. Mitre, M., Marlin, B.J., Schiavo, J.K., Morina, E., Norden, S.E., Hackett, T.A., Aoki, C.J., Chao, M.V., and Froemke, R.C. (2016). A Distributed Network for Social Cognition Enriched for Oxytocin Receptors. J. Neurosci. *36*, 2517–2535. https://doi.org/10.1523/JNEUROSCI.2409-15.2016.
50. Zhang, J., Li, S.J., Miao, W., Zhang, X., Zheng, J.J., Wang, C., and Yu, X. (2021). Oxytocin Regulates Synaptic Transmission in the Sensory Cortices in a Developmentally Dynamic Manner. Front. Cell. Neurosci. *15*, 673439. https://doi.org/10.3389/fncel.2021.673439.
51. Salahpour, A., Espinoza, S., Masri, B., Lam, V., Barak, L.S., and Gainetdinov, R.R. (2012). BRET biosensors to study GPCR biology, pharmacology, and signal transduction. Front. Endocrinol. *3*, 105. https://doi.org/10.3389/fendo.2012.00105.
52. Gales, C., Rebois, R.V., Hogue, M., Trieu, P., Breit, A., Hebert, T.E., and Bouvier, M. (2005). Real-time monitoring of receptor and G-protein interactions in living cells. Nat. Methods *2*, 177–184. https://doi.org/10.1038/nmeth743.
53. Namkung, Y., Le Gouill, C., Lukashova, V., Kobayashi, H., Hogue, M., Khoury, E., Song, M., Bouvier, M., and Laporte, S.A. (2016). Monitoring G protein-coupled receptor and beta-arrestin trafficking in live cells using enhanced bystander BRET. Nat. Commun. *7*, 12178. https://doi.org/10.1038/ncomms12178.
54. Schihada, H., Shekhani, R., and Schulte, G. (2021). Quantitative assessment of constitutive G protein-coupled receptor activity with BRET-based G protein biosensors. Sci. Signal. *14*, eabf1653. https://doi.org/10.1126/scisignal.abf1653.
55. Namkung, Y., LeGouill, C., Kumar, S., Cao, Y., Teixeira, L.B., Lukasheva, V., Giubilaro, J., Simões, S.C., Longpré, J.M., Devost, D., et al. (2018). Functional selectivity profiling of the angiotensin II type 1 receptor using pathway-wide BRET signaling sensors. Sci. Signal. *11*, eaat1631. https://doi.org/10.1126/scisignal.aat1631.
56. Stauffer, T.P., Ahn, S., and Meyer, T. (1998). Receptor-induced transient reduction in plasma membrane PtdIns(4,5)P2 concentration monitored in living cells. Curr. Biol. *8*, 343–346. https://doi.org/10.1016/s0960-9822(98)70135-6.
57. Hancock, J.F., Cadwallader, K., Paterson, H., and Marshall, C.J. (1991). A CAAX or a CAAL motif and a second signal are sufficient for plasma membrane targeting of ras proteins. EMBO J. *10*, 4033–4039. https://doi.org/10.1002/j.1460-2075.1991.tb04979.x.
58. Masuho, I., Martemyanov, K.A., and Lambert, N.A. (2015). Monitoring G Protein Activation in Cells with BRET. Methods Mol. Biol. *1335*, 107–113. https://doi.org/10.1007/978-1-4939-2914-6_8.
59. Gurevich, V.V., and Gurevich, E.V. (2019). GPCR Signaling Regulation: The Role of GRKs and Arrestins. Front. Pharmacol. *10*, 125. https://doi.org/10.3389/fphar.2019.00125.
60. Kohout, T.A., Lin, F.S., Perry, S.J., Conner, D.A., and Lefkowitz, R.J. (2001). beta-Arrestin 1 and 2 differentially regulate heptahelical receptor signaling and trafficking. Proc. Natl. Acad. Sci. USA *98*, 1601–1606. https://doi.org/10.1073/pnas.98.4.1601.
61. Zhang, M., Liu, X., Zhang, Y., and Zhao, J. (2010). Loss of betaarrestin1 and betaarrestin2 contributes to pulmonary hypoplasia and neonatal lethality in mice. Dev. Biol. *339*, 407–417. https://doi.org/10.1016/j.ydbio.2009.12.042.
62. Moo, E.V., van Senten, J.R., Bräuner-Osborne, H., and Møller, T.C. (2021). Arrestin-Dependent and -Independent Internalization of G Protein-Coupled Receptors: Methods, Mechanisms, and Implications on Cell Signaling. Mol. Pharmacol. *99*, 242–255. https://doi.org/10.1124/molpharm.120.000192.
63. Xiang, G., Acosta-Ruiz, A., Radoux-Mergault, A., Kristt, M., Kim, J., Moon, J.D., Broichhagen, J., Inoue, A., Lee, F.S., Stoeber, M., et al. (2022). Control of $G\alpha_q$ signaling dynamics and GPCR cross-talk by GRKs. Sci. Adv. *8*, eabq3363. https://doi.org/10.1126/sciadv.abq3363.
64. Abreu, N., Acosta-Ruiz, A., Xiang, G., and Levitz, J. (2021). Mechanisms of differential desensitization of metabotropic glutamate receptors. Cell Rep. *35*, 109050. https://doi.org/10.1016/j.celrep.2021.109050.
65. Lodowski, D.T., Pitcher, J.A., Capel, W.D., Lefkowitz, R.J., and Tesmer, J.J.G. (2003). Keeping G proteins at bay: a complex between G protein-coupled receptor kinase 2 and Gbetagamma. Science *300*, 1256–1262. https://doi.org/10.1126/science.1082348.
66. Lowe, J.D., Sanderson, H.S., Cooke, A.E., Ostovar, M., Tsisanova, E., Withey, S.L., Chavkin, C., Husbands, S.M., Kelly, E., Henderson, G., and Bailey, C.P. (2015). Role of G Protein-Coupled Receptor Kinases 2 and 3 in mu-Opioid Receptor Desensitization and Internalization. Mol. Pharmacol. *88*, 347–356. https://doi.org/10.1124/mol.115.098293.
67. Uehling, D.E., Joseph, B., Chung, K.C., Zhang, A.X., Ler, S., Prakesch, M.A., Poda, G., Grouleff, J., Aman, A., Kiyota, T., et al. (2021).

Design, Synthesis, and Characterization of 4-Aminoquinazolines as Potent Inhibitors of the G Protein-Coupled Receptor Kinase 6 (GRK6) for the Treatment of Multiple Myeloma. J. Med. Chem. *64*, 11129–11147. https://doi.org/10.1021/acs.jmedchem.1c00506.

68. Hanyaloglu, A.C., and von Zastrow, M. (2008). Regulation of GPCRs by endocytic membrane trafficking and its potential implications. Annu. Rev. Pharmacol. Toxicol. *48*, 537–568. https://doi.org/10.1146/annurev.pharmtox.48.113006.094830.
69. Tian, X., Kang, D.S., and Benovic, J.L. (2014). β-arrestins and G protein-coupled receptor trafficking. Handb. Exp. Pharmacol. *219*, 173–186. https://doi.org/10.1007/978-3-642-41199-1_9.
70. Shikanai, M., Ito, S., Nishimura, Y.V., Akagawa, R., Fukuda, M., Yuzaki, M., Nabeshima, Y.I., and Kawauchi, T. (2023). Rab21 regulates caveolin-1-mediated endocytic trafficking to promote immature neurite pruning. EMBO Rep. *24*, e54701. https://doi.org/10.15252/embr.202254701.
71. Li, G., and Stahl, P.D. (1993). Structure-function relationship of the small GTPase rab5. J. Biol. Chem. *268*, 24475–24480.
72. Stenmark, H., Parton, R.G., Steele-Mortimer, O., Lütcke, A., Gruenberg, J., and Zerial, M. (1994). Inhibition of rab5 GTPase activity stimulates membrane fusion in endocytosis. EMBO J. *13*, 1287–1296. https://doi.org/10.1002/j.1460-2075.1994.tb06381.x.
73. Beautrait, A., Paradis, J.S., Zimmerman, B., Giubilaro, J., Nikolajev, L., Armando, S., Kobayashi, H., Yamani, L., Namkung, Y., Heydenreich, F.M., et al. (2017). A new inhibitor of the beta-arrestin/AP2 endocytic complex reveals interplay between GPCR internalization and signalling. Nat. Commun. *8*, 15054. https://doi.org/10.1038/ncomms15054.
74. He, Y., Liu, H., Yin, N., Yang, Y., Wang, C., Yu, M., Liu, H., Liang, C., Wang, J., Tu, L., et al. (2021). Barbadin Potentiates Long-Term Effects of Lorcaserin on POMC Neurons and Weight Loss. J. Neurosci. *41*, 5734–5746. https://doi.org/10.1523/JNEUROSCI.3210-20.2021.
75. Sundqvist, M., Holdfeldt, A., Wright, S.C., Møller, T.C., Siaw, E., Jennbacken, K., Franzyk, H., Bouvier, M., Dahlgren, C., and Forsman, H. (2020). Barbadin selectively modulates FPR2-mediated neutrophil functions independent of receptor endocytosis. Biochim. Biophys. Acta. Mol. Cell Res. *1867*, 118849. https://doi.org/10.1016/j.bbamcr.2020.118849.
76. Katz, A., Wu, D., and Simon, M.I. (1992). Subunits beta gamma of heterotrimeric G protein activate beta 2 isoform of phospholipase C. Nature *360*, 686–689. https://doi.org/10.1038/360686a0.
77. Harden, T.K., Waldo, G.L., Hicks, S.N., and Sondek, J. (2011). Mechanism of activation and inactivation of Gq/phospholipase C-beta signaling nodes. Chem. Rev. *111*, 6120–6129. https://doi.org/10.1021/cr200209p.
78. Busnelli, M., Saulière, A., Manning, M., Bouvier, M., Galés, C., and Chini, B. (2012). Functional selective oxytocin-derived agonists discriminate between individual G protein family subtypes. J. Biol. Chem. *287*, 3617–3629. https://doi.org/10.1074/jbc.M111.277178.
79. Netser, S., Haskal, S., Magalnik, H., and Wagner, S. (2017). A novel system for tracking social preference dynamics in mice reveals sex- and strain-specific characteristics. Mol. Autism. *8*, 53. https://doi.org/10.1186/s13229-017-0169-1.
80. Ahmad, M., Polepalli, J.S., Goswami, D., Yang, X., Kaeser-Woo, Y.J., Südhof, T.C., and Malenka, R.C. (2012). Postsynaptic complexin controls AMPA receptor exocytosis during LTP. Neuron *73*, 260–267. https://doi.org/10.1016/j.neuron.2011.11.020.
81. Bacaj, T., Ahmad, M., Jurado, S., Malenka, R.C., and Südhof, T.C. (2015). Synaptic Function of Rab11Fip5: Selective Requirement for Hippocampal Long-Term Depression. J. Neurosci. *35*, 7460–7474. https://doi.org/10.1523/JNEUROSCI.1581-14.2015.
82. Soler-Llavina, G.J., Arstikaitis, P., Morishita, W., Ahmad, M., Südhof, T.C., and Malenka, R.C. (2013). Leucine-rich repeat transmembrane proteins are essential for maintenance of long-term potentiation. Neuron *79*, 439–446. https://doi.org/10.1016/j.neuron.2013.06.007.
83. Troyano-Rodriguez, E., Wirsig-Wiechmann, C.R., and Ahmad, M. (2019). Neuroligin-2 Determines Inhibitory Synaptic Transmission in the Lateral Septum to Optimize Stress-Induced Neuronal Activation and Avoidance Behavior. Biol. Psychiatry *85*, 1046–1055. https://doi.org/10.1016/j.biopsych.2019.01.022.
84. Nagaraja, R.Y., Stiles, M.A., Sherry, D.M., Agbaga, M.P., and Ahmad, M. (2023). Synapse-Specific Defects in Synaptic Transmission in the Cerebellum of W246G Mutant ELOVL4 Rats-a Model of Human SCA34. J. Neurosci. *43*, 5963–5974. https://doi.org/10.1523/JNEUROSCI.0378-23.2023.
85. Troyano-Rodriguez, E., Mann, S., Ullah, R., and Ahmad, M. (2019). PRRT1 regulates basal and plasticity-induced AMPA receptor trafficking. Mol. Cell. Neurosci. *98*, 155–163. https://doi.org/10.1016/j.mcn.2019.06.008.
86. Shepherd, G.M.G., Pologruto, T.A., and Svoboda, K. (2003). Circuit analysis of experience-dependent plasticity in the developing rat barrel cortex. Neuron *38*, 277–289. https://doi.org/10.1016/s0896-6273(03)00152-1.
87. Huang, T., Guan, F., Licinio, J., Wong, M.L., and Yang, Y. (2021). Activation of septal OXTr neurons induces anxiety- but not depressive-like behaviors. Mol. Psychiatry *26*, 7270–7279. https://doi.org/10.1038/s41380-021-01283-y.
88. Perkins, K.L. (2006). Cell-attached voltage-clamp and current-clamp recording and stimulation techniques in brain slices. J. Neurosci. Methods *154*, 1–18. https://doi.org/10.1016/j.jneumeth.2006.02.010.
89. Alcami, P., Franconville, R., Llano, I., and Marty, A. (2012). Measuring the firing rate of high-resistance neurons with cell-attached recording. J. Neurosci. *32*, 3118–3130. https://doi.org/10.1523/JNEUROSCI.5371-11.2012.
90. Nunemaker, C.S., DeFazio, R.A., and Moenter, S.M. (2003). A targeted extracellular approach for recording long-term firing patterns of excitable cells: a practical guide. Biol. Proced. Online *5*, 53–62. https://doi.org/10.1251/bpo46.
91. Martin, E.E., Wleklinski, E., Hoang, H.T.M., and Ahmad, M. (2021). Interaction and Subcellular Association of PRRT1/SynDIG4 With AMPA Receptors. Front. Synaptic Neurosci. *13*, 705664. https://doi.org/10.3389/fnsyn.2021.705664.

STAR★METHODS

KEY RESOURCES TABLE

REAGENT or RESOURCE	SOURCE	IDENTIFIER
Antibodies		
Rabbit monoclonal anti-β-arrestin-1	Cell Signaling Technology	Cat# 30036; RRID:AB_2798985
Rabbit monoclonal anti-β-arrestin-2	Cell Signaling Technology	Cat# 3857; RRID:AB_2258681
Mouse monoclonal anti-GRK2	Santa Cruz Biotechnology	Cat# sc-13143; RRID:AB_626751
Rabbit monoclonal anti-GRK3	Cell Signaling Technology	Cat# 80362; RRID:AB_2799951
Mouse monoclonal anti-GRK5	Santa Cruz Biotechnology	Cat# sc-518005; RRID:N/A
Rabbit monoclonal anti-GRK6	Cell Signaling Technology	Cat# 5878; RRID:AB_11179210
Mouse monoclonal anti-β-actin	Millipore Sigma	Cat# A1978; RRID:AB_476692
Goat anti-Mouse IgG-IR800CW	LI-COR	Cat# 926-32210; RRID:AB_621842
Goat anti-Rabbit IgG -IR800CW	LI-COR	Cat# 926-32211; RRID:AB_621843
Goat anti-Rabbit IgG Alexa Flour 568nm	Thermo Fisher Scientific	Cat#A11011; RRID:AB_143157
Goat anti-Mouse IgG Alexa Flour 680nm	Jackson ImmunoResearch	Cat#115-625-146; RRID:AB_2338935
Goat anti-Rabbit IgG Alexa Flour 680nm	Jackson ImmunoResearch	Cat#111-625-144; RRID:AB_2338085
Bacterial and virus strains		
AAV.CMV.HI. eGFP-Cre.WPRE.SV40	Addgene	Cat#105545-AAV5
AAV2/8.U6.gArrb1.hSyn.eGFP	Vector Builder	N/A
AAV2/5.hSyn.ChR2(H134R)-eYFP	University of Pennsylvania	Addgene26973P
Lentivirus: L301Syn nanoLuc−PH-PLCδ	This Paper	N/A
Lentivirus: L301HaloTag-CAAX	This Paper	N/A
Lentivirus: L301Syn HA-OXTR-nanoLuc	This Paper	N/A
Lentivirus: L301 β-arrestin-1-HaloTag	This Paper	N/A
Lentivirus: L301β−arrestin-2-HaloTag	This Paper	N/A
Lentivirus: L301GRK2-HaloTag	This Paper	N/A
Lentivirus: L301GRK3-HaloTag	This Paper	N/A
Lentivirus: L301GRK5-HaloTag	This Paper	N/A
Lentivirus: L301GRK6-HaloTag	This Paper	N/A
Lentivirus: L301HaloTag-Rab5	This Paper	N/A
Lentivirus: L301HaloTag-Rab11	This Paper	N/A
Lentivirus: L301HaloTag-Rab21	This Paper	N/A
Lentivirus: L301HA-Rab5 DN	This Paper	N/A
Chemicals, peptides, and recombinant proteins		
Oxytocin	Tocris	Cat#1910, CAS: 50-56-6
(Thr^4,Gly^7)-Oxytocin (TGOT)	Bachem	Cat#4013837, CAS: 60786-59-6
SR49059	Cayman Chemical	Cat#17972, CAS: 150375-75-0
(d(CH$_2$)$_5$^{1},Tyr(Me)^2,Arg^8)-Vasopressin	Tocris	Cat#3377, CAS: 73168-24-8
FR900359 (UBO-QIC)	Cayman Chemical	Cat#33666, CAS: 107530-18-7
Tetrodotoxin	Cayman Chemical	Cat#14964, CAS: 18660-81-6
NBQX	Cayman Chemical	Cat#14914, CAS: 479347-86-9
Picrotoxin	Sigma	Cat# P1675-5G, CAS: 124-87-8
Gallein	Tocris	Cat#3090, CAS: 2103-64-2
CMPD101	Cayman Chemical	Cat#26808, CAS: 865608-11-3

(*Continued on next page*)

Continued

REAGENT or RESOURCE	SOURCE	IDENTIFIER
Barbadin	MedChemExpress	Cat# HY-119706, CAS: 356568-70-2
GRK6-IN-1	MedChemExpress	Cat# HY-142812, CAS: 2677786-61-5
GRK6-IN-2	MedChemExpress	Cat# HY-142817, CAS: 2677786-27-3
Critical commercial assays		
NanoBRET HaloTag 618 Ligand	Promega	Cat# G9801
NanoBRET Nano-Glo Substrate	Promega	Cat# N1571
NanoBRET Nano-Glo Detection Systems	Promega	Cat# N1661
Experimental models: Cell lines		
HEK293	ATCC	CRL-1573
Experimental models: Organisms/strains		
Mouse: *Oxtr*$^{tm1(cre/GFP)Rpa}$/J	The Jackson Laboratory	Stock #030543; RRID: IMSR_JAX: 030543
Mouse: *C57BL6/J*	The Jackson Laboratory	Stock #000664; RRID:IMSR_JAX:000664
Mouse: *B6.Cg-Gt(ROSA)26Sor*$^{tm14(CAG-tdTomato)Hze}$/J	The Jackson Laboratory	Stock #007914; RRID: IMSR_JAX: 007914
Mouse: *B6.129X1(Cg)-Arrb1*^{tm1Jse}/J	The Jackson Laboratory	Stock #011131; RRID:IMSR_JAX:011131
Mouse: *Arrb2*^{tm1Rjl}/J	The Jackson Laboratory	Stock #011130; RRID: IMSR_JAX: 011130
Mouse: *B6J.129(B6N)-Gt(ROSA)26Sor*$^{tm1(CAG-cas9*,-EGFP)Fezh}$/J	The Jackson Laboratory	Stock #026175; RRID: IMSR_JAX: 026175
Oligonucleotides		
tgtgcggctagtcatccgga-g*Arrb1*	This Paper	N/A
Recombinant DNA		
L301Syn nanoLuc−PH-PLCδ	This Paper	PH-PLCδ sequence from Addgene #21179
L301HaloTag-CAAX	This Paper	CAAX sequence from Addgene #79574
L301HaloTag-2x FYVE	This Paper	2xFYVE sequence from Addgene #140047
L301Syn HA-OXTR-nanoLuc	This Paper	OXTR, GenBank: NM_001081147
L301 β-arrestin-1-HaloTag	This Paper	β-arrestin-1, GenBank: NM_177231
L301β-arrestin-2-HaloTag	This Paper	β-arrestin-2, GenBank: NM_001271358
L301GRK2-HaloTag	This Paper	GRK2, GenBank: NM_001290818
L301GRK3-HaloTag	This Paper	GRK3, GenBank: NM_177078
L301GRK5-HaloTag	This Paper	GRK5, GenBank: NM_018869
L301GRK6-HaloTag	This Paper	GRK6, GenBank: NM_001004106
L301HaloTag-Rab5	This Paper	Rab5, GenBank: NM_004162
L301HaloTag-Rab11	This Paper	Rab11, GenBank: NM_004663
L301HaloTag-Rab21	This Paper	Rab21, GenBank: NM_014999
L301HA-Rab5 DN	This Paper	N/A
Software and algorithms		
Mini Analysis	Synaptosoft, Inc.	http://www.synaptosoft.com/MiniAnalysis/
GraphPad Prism	Graphpad	https://www.graphpad.com/scientific-software/prism/
Igor Pro with Custom package	Igor Pro	https://www.wavemetrics.com/
Fiji (ImageJ)	NIH	https://imagej.nih.gov/ij/
NIS Elements Viewer	Nikon	https://www.microscope.healthcare.nikon.com/products/software/nis-elements/viewer
Microsoft Office	Microsoft Office	https://www.office.com/
BioRender	BioRender	https://www.biorender.com/

RESOURCE AVAILABILITY

Lead contact

Further information and requests for resources and reagents should be directed to and will be fulfilled by the lead contact: Mohiuddin Ahmad (Mohiuddin-Ahmad@ouhsc.edu).

Materials availability

Requests for resources and reagents will be fulfilled by the lead contact with a completed Materials Transfer Agreement.

Data and code availability

- This study did not generate large-scale datasets.
- No original code was generated in this study.
- Any additional information required to reanalyze the data reported in this paper is available from the lead contact upon request.

EXPERIMENTAL MODEL AND STUDY PARTICIPANT DETAILS

All animal procedures were approved by the Institutional Animal Care and Use Committee of the University of Oklahoma Health Sciences Center (21-014-SCHI). Animals were housed in a pathogen-free barrier animal facility of the University of Oklahoma Health Sciences Center. The housing room was maintained in a dark/light cycle of 12:12 h with lights on at 6 a.m. Food and water were provided *ad-libitum*. Breeding pairs were established, and the genotypes were confirmed by PCR with specific primers. *Arrb1*$^{-/-}$ (stock no: 011131), *Arrb2*$^{-/-}$ (stock no: 011130), *Rosa26-LSL-Cas9* (stock no: 026175), Oxtr-IRES-Cre (stock number: 030543), Ai14 (stock number: 007914), and C57BL/6J animals were obtained from the Jackson Laboratory. Mice belonging to both sexes in the age range of 3–9 months were used in the experiments.

METHOD DETAILS

Plasmids and viral vectors

The guide RNA (gRNA) sequences targeting mouse *Arrb1* (six in number) were selected using web based CRISPOR and cloned after the U6 promoter into LentiCrisprV2 mammalian expression vector. The ability of each gRNA to silence mouse *Arrb1* was tested in HEK293 cells by co-transfection of the gRNA and spCas9-expressing vector with a plasmid expressing mouse HA-tagged β-arrestin-1. The efficiency of knockout was examined on immunoblots of HEK293 cell lysates labeled with a β-arrestin-1 antibody. The gRNA causing the most effective deletion (tgtgcggctagtcatccgga) was cloned into an adeno-associated virus (AAV) shuttle vector. Purified and concentrated preparations of AAV2/8-g*Arrb1* were custom-made by Vector Builder. The AAV2/5-CMV-HI-Cre-GFP was obtained from Addgene.

To generate lentiviral expression vector L301Syn nanoLuc−PH-PLCδ, the pleckstrin homology domain of PLCδ was synthesized as a gBlock gene fragment (Integrated DNA technologies) and cloned in frame after nanoluciferase sequence (Promega) in a custom lentiviral vector L301. The L301HaloTag-CAAX vector was generated by PCR amplification of HaloTag sequence from pHTN HaloTag CMV-neo (Promega) and cloned in frame before the CAAX box sequence from Ras. The L301Syn HA-OXTR-nanoLuc vector was produced by PCR amplification of Oxtr cDNA from mouse brain cDNA using gene-specific primers and cloned before nanoluciferase sequence derived from pNLF1N CMV-Hygro plasmid (Promega). We generated the L301 β-arrestin-1-HaloTag, β-arrestin-2-HaloTag, GRK2-HaloTag, and GRK3-HaloTag vectors by amplifying the respective cDNA from mouse brain cDNA using gene-specific primers and cloning before the HaloTag sequence in L301. L301 GRK5-HaloTag, GRK6-HaloTag, HaloTag-Rab5 and HaloTag-Rab21 were made by amplifying cDNA from mammalian expression plasmids and cloning before/after the HaloTag sequence. The transcripts are driven by the human synapsin promoter in L301Syn vectors, and by the ubiquitin c promoter in L301 vectors. Third-generation lentiviral preparations were made using standard methods as described before.[80,81]

Stereotaxic surgery

The administration of AAV in the mouse brain LS was performed using a stereotaxic apparatus coupled to a digital display console (Model 922, David Kopf Instruments). The animals were anesthetized with intraperitoneal injection of a mixture of ketamine (75 mg/kg body weight) and dexmedetomidine (0.375 mg/kg body weight) and immobilized on the stereotaxic apparatus.[80,82,83] Unilateral perforations were made in the skull and a glass cannula was lowered into the LS (coordinates: bregma, +0.8 mm; lateral, 0.35 mm; ventral, 3.0 mm from dura).[83] Approximately 0.5–0.7 μL of virus (~10^{12} GC/mL) was injected using a microinjection pump (Model AL-1000, World Precision Instruments) at a flow rate of 0.1 μL/min. After the injections, the cannula was slowly withdrawn. The scalp was then sealed with a tissue adhesive (3M Vetbond, 3M Animal Care Products), and atipamezole (10 mg/kg body weight) was injected by intraperitoneal injection to reverse the effect of dexmedetomidine. Carprofen (5 mg/kg body weight) was administered subcutaneously before surgery to relieve pain in the perioperative period.

Electrophysiological recordings

Acute coronal slices containing LS, PFC or BNST were prepared from adult mouse brains of both sexes. Following anesthesia with ketamine and dexmedetomidine, animals were transcardially perfused with ice-cold dissection buffer containing (in mM): 50 sucrose, 125 NaCl, 25

$NaHCO_3$, 2.5 glucose, 2.5 KCl, 1.25 NaH_2PO_4, 4.9 $MgCl_2$ and 0.1 $CaCl_2$.[83,84] The mice were decapitated, and their brains rapidly removed. 250 μm thick slices were cut on a vibratome (VT1200S, Leica Biosystems) in the dissection buffer, and immediately transferred to an incubation chamber which had artificial cerebrospinal fluid (ACSF) containing (in mM): 119 NaCl, 26 $NaHCO_3$, 11 glucose, 2.5 KCl, 1 NaH_2PO_4, 1.3 $MgSO_4$ and 2.5 $CaCl_2$.[80,83,85] The slices were allowed to recover at 32°C for 30 min before being allowed to equilibrate at room temperature for a minimum 1 h. The slices were placed in a recording chamber constantly perfused (1.5–2.0 mL/min) with heated ACSF (26°C–28°C) and gassed continuously with 95% O2 and 5% CO2. The drugs were bath applied in ACSF at indicated concentrations. For spontaneous IPSC (sIPSC) and mEPSC recordings, whole-cell patch pipettes (2–4 MΩ) were filled with a solution containing (in mM): 117.5 $CeMeSO_3$, 15.5 CsCl, 10 TEACl, 8 NaCl, 1 $MgCl_2$, 10 HEPES, 0.5 EGTA, 4 Mg_2ATP, 0.3 Na_3GTP, 10 phosphocreatine and 1 QX-314 Chloride (pH 7.25–7.3; osmolality 300–305 mOsm/kg). For cell-attached loose-seal recordings, pipettes were filled with 150 mM NaCl. The neurons were visualized using infrared differential interference contrast (DIC) on an upright microscope (Olympus BX51WI, Olympus) and tdTomato containing neurons were identified using a fluorescence illumination system (Lumen 200, Prior Scientific). Whole-cell patch-clamp recordings were done in voltage-clamp mode, holding the cells at 0 mV for sIPSC and at −65 mV for mEPSC. Cell-attached, loose-seal (<100 MΩ) recordings were done in voltage-clamp mode to record spikes.[16,86,87] Compared to the giga-seal, the loose-seal configuration produces less damage to the cell membrane, more stable spike recordings, and larger spike amplitudes.[88–90] The voltage was adjusted, if needed, to keep the baseline current close to 0 pA to prevent any change in resting membrane potential.[88] Recording traces of 10 s duration were acquired sequentially. The frequency of synaptic events and spikes was calculated for each trace by counting the number of events and dividing them by the length of the trace (10 s). The frequency of events was plotted against time to obtain the time course. For bar graphs of electrophysiological data, three or five such data points were averaged to calculate the peak and baseline respectively. Data were collected with MultiClamp 700B amplifier (Molecular Devices), filtered with 2 kHz Bessel filter and digitized at 10 kHz with the A/D converter ITC-18 (Instrutech Corporation). Data were acquired and analyzed using a custom-made program written in Igor Pro software (Wavemetrics).[80,84]

Immunohistochemistry and immunoblotting

For immunohistochemistry, animals were anesthetized with a mixture of ketamine and dexmedetomidine as above. The animals were then transcardially perfused with phosphate-buffered saline (PBS, Sigma) for 2 min followed by 4% paraformaldehyde (PFA, Sigma) in PBS at a rate of 1.5 mL/min for 20 min. Brains were removed and placed in the 4% PFA solution overnight. Brains were washed the next day with PBS and 40 μm thick slices were cut on a vibratome (VT1000S, Leica Biosystems). Free-floating slices were incubated in a blocking solution containing 3% normal goat serum and 0.3% Triton X-100 in PBS for 1 h at room temperature.[83] The slices were then incubated with primary antibody against β-arrestin-1 (Cell Signaling, Cat# 30036) in the blocking buffer overnight and subsequently secondary antibody (goat anti-rabbit Alexa 568, Thermo Fisher Scientific) was applied for 1 h at room temperature, spaced with multiple PBS washes. The slices were mounted on glass slides in Fluoromount-G (Southern Biotech) mounting medium. The images were acquired with 10× or 60× objectives on laser-scanning (Olympus) or spinning-disk (Nikon) confocal microscopes.

For immunoblotting, acute brain slices containing the LS were prepared as described for electrophysiology. The slices were lysed in RIPA buffer containing 150 mM NaCl, 50 mM Tris (pH 7.4), 2 mM EDTA, 1% Triton X-100, 0.5% sodium deoxycholate, 0.1% SDS and protease inhibitors (Roche). The lysate was incubated on ice for 30 min followed by centrifugation at 16,000 g for 20 min at 4°C. The supernatant was collected and protein quantification was performed using the BCA assay. The supernatant (20–75 μg protein) was mixed with sample buffer containing 10% β-mercaptoethanol and incubated for 3 min at 95°C. The samples were loaded on to Bolt Bis-Tris Plus gels (Thermo Fisher Scientific), transferred to nitrocellulose membranes (Licor) and immunoblotted with indicated primary antibodies for 2 h at room temperature. After incubation with appropriate secondary antibodies, the membranes were imaged on an Odyssey Imaging System (LI-COR) using the Image Studio acquisition program (LI-COR). The following primary antibodies were used: β-arrestin-1 (Cell Signaling, Cat# 30036), β-arrestin-2 (Cell Signaling, Cat# 3857), GRK2(Santa Cruz Biotechnology, Cat# sc-13143), GRK3(Cell Signaling, Cat# 80362) GRK5(Santa Cruz Biotechnology, Cat# sc-518005), GRK6(Cell Signaling, Cat# 5878) and β-actin (Millipore Sigma, Cat# A1978). The secondary antibodies that were used: IR800-conjugated goat anti-mouse and goat anti-rabbit (LI-COR); Alexa Fluor 680-conjugated goat anti-mouse and goat anti-rabbit (Jackson Immunoresearch) immunoglobulins.

Primary neuronal cultures

Primary neuronal cultures were prepared from E17-E18 C57BL6/J mice.[80,91] Cortical (neocortical and hippocampal) tissue was dissected out from brains and incubated with a digestion solution containing trypsin for 15 min at 37°C. The tissue was triturated in plating medium containing Neurobasal plus medium, 2% B27 plus supplement, 2 mM GlutaMAX and 5% heat-inactivated horse serum (all from Thermo Fisher Scientific). The cells were plated in poly-L-lysine (Sigma) coated wells in opaque 96-well plates at a density of 120,000 cells per mL of the plating medium. On the 4th day after plating, the medium was replaced with a maintenance medium containing Neurobasal plus medium, 2% B27 plus supplement, and 2 mM GlutaMAX. FUDR was added to block glial growth at this time point. Half of the medium in each well was replaced with fresh medium every 3–4 days. Lentivirus preparations were applied to the cultures on day in vitro (DIV) 8 and the experiments were done on cultures at DIV16.

Bioluminescence Resonance Energy Transfer (BRET)

Primary cortical neuronal cultures were seeded at 120,000 cells/mL in a 96-well white plate (Costar) and incubated at 37°C, 5% CO2, day in vitro (DIV) 0. Lentivirus transduction was performed at DIV 10–12. A week after transduction, the primary cortical neuronal

cultures (DIV 16–18) were incubated overnight in the absence and presence of NanoBRET HaloTag 618 Ligand (Promega, Cat.#G9801 or part of N1661) to a 100 nM final concentration. Next day, inhibitors or DMSO were added to the cells and incubated at 37°C, 5% CO2 for 30 min. 5× solution of NanoBRET Nano-Glo Substrate (Promega, Cat.#N1571 or part of N1661) was prepared from 100-fold dilution of the stock then added to neuronal culture and incubated for 5 min at room temperature. The donor and acceptor emissions were measured at 450 nm and 610 nm respectively in an Agilent Biotek Synergy *Neo*2 plate reader, sampling every 10 s. The baseline signal was collected for 4 min followed by agonist application to 200 nm final concentration. We calculated BRET ratio = (Emission610/Emission 450) $_{\text{HT ligand}}$ - (Emission610/Emission 450) $_{\text{no HT ligand}}$. ΔBRET was obtained by subtracting the averaged baseline from all values, and normalized BRET was calculated by dividing all values by averaged baseline. The data were plotted in GraphPad Prism v9.5.1.

Drugs

The following drugs were kept at −20°C as stock solutions and dissolved in ACSF or cell culture media to the final concentration on the day of experiments. Oxytocin (1910, Tocris), (Thr^4,Gly^7)-Oxytocin (TGOT) (4013837, Bachem), SR49059 (17972, Cayman Chemical, (d(CH$_2$)$_5$^{1},Tyr(Me)^2,Arg^8)-Vasopressin (3377,Tocris), FR900359 (UBO-QIC) (33666, Cayman Chemical) Tetrodotoxin (14964, Cayman Chemical) NBQX (14914, Cayman Chemical), Picrotoxin (P1675-5G, Sigma), Gallein (3090,Tocris), CMPD101 (26808, Cayman Chemical), Barbadin (HY-119706, MedChemExpress), GRK6-IN-1 (HY-142812, MedChemExpress), and GRK6-IN-2 (HY-142817, MedChemExpress) were purchased from vendors as indicated.

QUANTIFICATION AND STATISTICAL ANALYSIS

Statistical analysis was performed using Student's t test when comparing two groups (Figures 5D, 5E, S2D, and S4D). Repeated Measures one-way ANOVA followed by Tukey's multiple comparison post-hoc test was used for data consisting of three matched measures (baseline, first response, and second response) from each cell (Figures 1A–1F, 2A–2C, S2A, S2C, S3A, and S3B). Regular one-way ANOVA with Dunnett's post-hoc test (for comparison with control) or Tukey's multiple comparison post-hoc test (for multiple comparisons) was used for unpaired/unmatched data from more than two groups (Figures 5F, S4A, S4B, S9A, and S9B). Repeated Measures two-way ANOVA followed by Tukey's multiple comparison post-hoc test was used for data consisting of two independent variables, the matched measures (baseline, first response, and second response) from each cell and the genotype (Figures 4H and S4C). The analyses were done in GraphPad Prism 10. Data are displayed as mean ± SEM. Statistical significance was set to $^*p < 0.05$, $^{**}p < 0.01$, $^{***}p < 0.001$, $^{****}p < 0.0001$. The applied statistical tests are additionally indicated for each set of data in the figure legends. The details of statistical analyses are provided in the Supplementary Excel file (Table S1).